Journal of Marine Systems 78 (2009) S205–S226

Contents lists available at ScienceDirect

Journal of Marine Systems

journal homepage: www.elsevier.com/locate/jmarsys

Eddies and filaments of the Western Adriatic Current near Cape Gargano: Analysis and prediction

D.M. Burrage *, J.W. Book, P.J. Martin

Ocean Sciences Branch, Naval Research Laboratory, Stennis Space Center, 39529, MS, USA

ARTICLE INFO

Article history:
Received 31 March 2008
Received in revised form 21 October 2008
Accepted 22 January 2009
Available online 9 March 2009

Keywords:
Eddies
Filaments
Upwelling
Temperature
Salinity
Chlorophyll
Italy, Central Adriatic Sea
(Lat. 40–44°N., Long. 14–19°E)

ABSTRACT

Remote sensing and in situ observations, and model simulations made during the Dynamics of the Adriatic in Real Time (DART) project in the central Adriatic Sea during 2006 reveal intense mesoscale eddy activity in the West Adriatic Current (WAC) system, that flows along the Italian coast. We investigate the origin, scale and rate of evolution of these features, and consider their potential contributions to across-shelf exchange, as a basis for planning future operational coastal prediction and monitoring programs. Predictions from a regional Adriatic Sea implementation of the Navy Coastal Ocean Model (NCOM) are assessed using observations from satellites, current meter moorings, and ship hydrographic transects.

Near Cape Gargano in summer, mesoscale eddies and filaments observed in remote sensing imagery and in situ data exhibit horizontal and vertical scales of about 30 km and 25 m, respectively. The observed eddies develop along the WAC front under transient wind conditions, while a quasi-permanent anti-cyclonic circulation appears downstream of the cape. NCOM model predictions show that well-organized, multiple-eddy features appear, grow in unison, then dissipate along the coast west of Cape Gargano in response to transient along-shelf wind forcing, while east of it individual eddies are generated by interaction of the WAC main stream with the bathymetry surrounding the cape. The eddies evolve over time scales of a few days to a week in response to forcing transients. Moderate to strong northwest winds compress the WAC coastward and suppress the instabilities, while relaxing northwest winds or shifts to southeast winds expand the WAC and enhance instability growth. Together with entrained filaments of coastal water, the eddies translate, stretch and rotate in response to WAC horizontal advection and shear. The qualitative character and evolution of the modeled features agree with the observations, and model statistics reveal patterns of variability on monthly and seasonal time scales that are consistent with the appearance of individual eddies in both the model results and observations.

In the model, patterns of upwelling and downwelling associated with the WAC main stream and eddies may be linked to dynamical characteristics of the WAC flow and specific bathymetric features. Under wintertime conditions, theoretical arguments predict an upwelling response as flow divergence changes absolute vorticity where the WAC rounds the cape, while Ekman pumping driven by surface winds or bottom stress and associated secondary circulation could explain upwelling and downwelling patches appearing around the rims of individual eddies. The upwelling dynamics are complicated by seasonal stratification effects and bathymetric features, and more work is needed to elucidate these processes.

Based on their frequent occurrence, large size compared to the shelf width, high intensity and current shear, and secondary circulations, the eddies and filaments could contribute significantly to across-shelf exchange and coastal/deep-ocean mixing, with important implications for coastal monitoring and prediction. Their generation and evolution present special challenges for coastal prediction, but our results demonstrate that combined use of remote sensing imagery and numerical model simulations can yield valuable insight into such processes, and thereby help plan future monitoring and prediction efforts.

Published by Elsevier B.V.

1. Introduction

The circulation of the Adriatic Sea is characterized by a complex interplay between its bathymetry, seasonal and spring time river inflows and time-varying winds (Orlić et al., 1992; Cushman-Roisin, 2001; Korotenko, 2007). The bathymetry consists of a relatively deep basin to the south, the ~1200-m deep South Adriatic Pit (SAP), separated from a shallower depression, the ~270-m deep Middle

* Corresponding author. Code 7332, Oceanography Branch, Naval Research Laboratory, Stennis Space Center, MS 39529, USA. Tel.: +1 228 688 5241; fax: +1 228 688 5997.

E-mail addresses: burrage@nrlssc.navy.mil (D.M. Burrage), book@nrlssc.navy.mil (J.W. Book), martin@nrlssc.navy.mil (P.J. Martin).

0924-7963/$ – see front matter. Published by Elsevier B.V.
doi:10.1016/j.jmarsys.2009.01.024

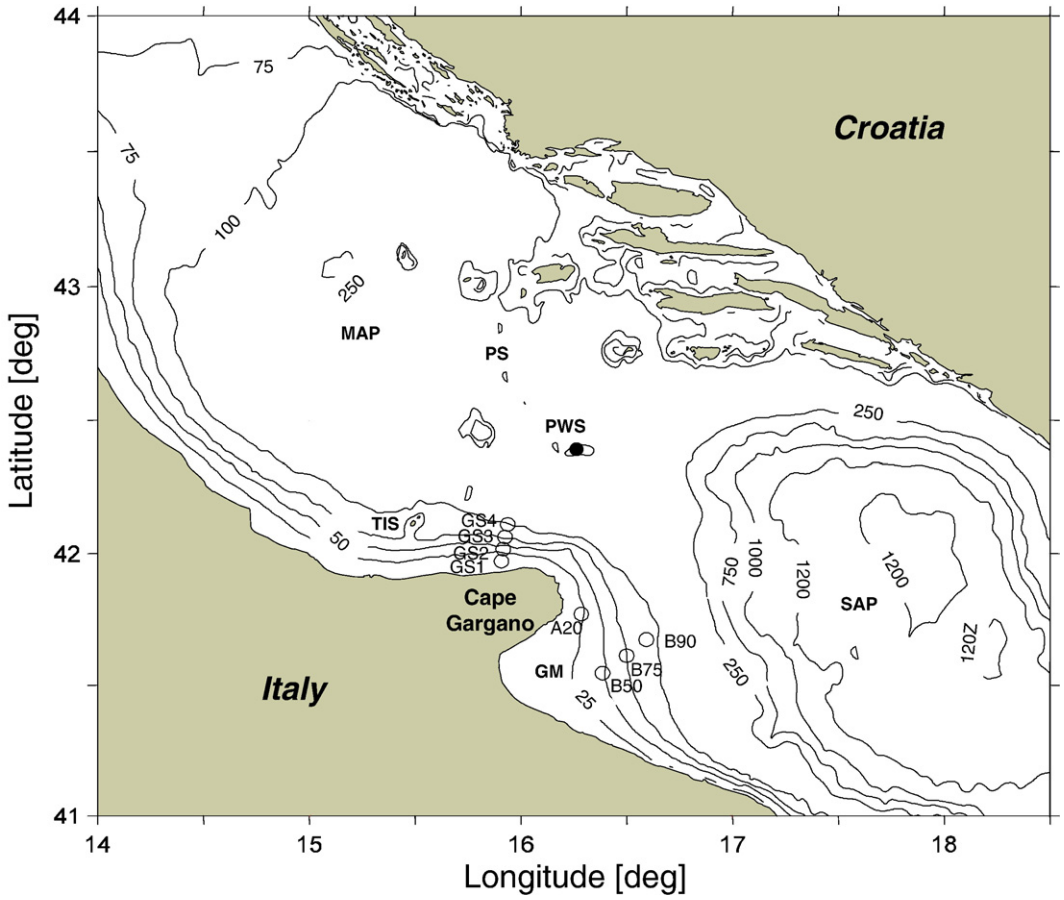

Fig. 1. Regional domain with bathymetry. Topographic features include the Middle (MAP), South Adriatic Pit (SAP), Palagruzza Sill (PS), Tremiti Islands group (TIS) and Gulf of Manfredonia (GM). The location of current meter moorings GS1–4, A20, B50, B75 and B90 (open circles) and the Palagruzza weather station, located on Palagruzza Island (PWS, closed circle) are also indicated. Contour depth labels are in meters. Additional moorings deployed further along the GS line that spanned the central Adriatic during DART are not shown.

Adriatic Pit (MAP), in the central region by the (<200 m) deep Palagruzza Sill (Fig. 1). There is a moderately deep passage into the Ionian Sea through the Strait of Otranto to the southeast, and a gradual shoaling to the northwest. The seasonal discharge of most rivers flowing into the Adriatic Sea has been estimated (Raicich, 1994), but daily discharge figures are only readily available for the Po River. The mean annual runoff of all these rivers is 5.7×10^3 m^3 s^{-1}. The Po River, which is the largest, has a mean annual runoff of about 1.6×10^3 m^3 s^{-1} and a spring maximum of 3.4×10^3 m^3 s^{-1} (Raicich, 1994, 1996). Relatively weak summer winds are interrupted by short periods of strong northeast (bora) and southeast (sirocco) winds, which recur more frequently in winter (Cushman-Roisin et al., 2001).

The circulation is predominantly cyclonic, with the East Adriatic Current (EAC) flowing northwest along the Albanian and Croation coasts and the West Adriatic Current (WAC) flowing southeast along the Italian coast. The overall cyclonic circulation of the Adriatic has several smaller cyclonic gyres embedded in it (Poulain, 2001), the most notable being the topographically-controlled flow that forms the perimeter of the South Atlantic Gyre (SAG) and follows the sloping wall of the SAP. The WAC, our main focus, is a relatively fresh meandering stream carrying low salinity coastal water strongly augmented by the Po River, which discharges into the northwest Adriatic. The WAC is separated from the circulation in the interior by a more or less sharp (depending upon season) temperature, salinity and hence density front roughly paralleling, but frequently expanding seaward of, the 40-m isobath.

Satellite imagery, augmented by in situ mooring data at selected locations, reveals a rich spectrum of ocean mesoscale (50–500 km) and sub-mesoscale flow (5–50 km) features associated with the Adriatic Sea circulation (for simplicity, we adopt the term mesoscale in this paper to span both these scales). Cushman-Roisin et al. (2007) and Korotenko (2007) have successfully modeled several characteristic mesoscale features including eddies and jets associated with spatially varying winds (predominantly bora), and the Triple Meander (TM) and Rimini Squirt (RS), which Korotenko (2007) argues result from (quasi-linear) instabilities associated with larger-scale flow disturbances in the WAC front. The RS flows transverse to the WAC, and forms a mushroom-like current (a jet terminated by a pair of cyclonic and anti-cyclonic eddies). A similar but stronger feature located in the MAP region north of Cape Gargano was also identified in Korotenko's model simulations. His model results gave useful indications of the temporal scales of variability of these features, which may evolve and dissipate on time scales varying from one day to several weeks, and they demonstrated that the onset or relaxation of spatially varying wind fields plays a significant role in the generation, maintenance and dissipation of these instabilities.

This brief review raises a number of questions concerning the mesoscale variability of the WAC such as: Where do the WAC eddies and filaments form? How fast do they evolve? What drives them? Are they predictable? Do they cause significant across-shelf exchange? In an attempt to address some of these questions, we analyze a combination of remote sensing, in situ and model data, look for recurring mesoscale features or patterns, assess the model predictions, and draw inferences regarding the associated time-varying forcings and response.

During 2005–6, the U.S. Naval Research Laboratory (NRL), in collaboration with the NATO Undersea Research Centre (NURC) and many other international partners, undertook a study to evaluate monitoring and prediction capabilities for vigorous, swiftly-evolving fronts and eddies in a topographically-controlled coastal environment. The Palagruzza Sill and Cape Gargano area of the central

Adriatic Sea were chosen as the focus areas during the Dynamics of the Adriatic in Real-Time (DART) project, since they exhibit strong isobath curvature and divergence associated with sharp topographic changes and the WAC frontal system produces instabilities in this region (e.g., see Plate 1 in Cushman-Roisin et al., 2001). A major part of the NRL component of the DART experiments was the deployment of 12 bottom-mounted, upward-looking Acoustic Doppler Current Profiler (ADCP) moorings spanning the Palagruzza Sill from the north shore of Cape Gargano, Italy to the Croatian Island of Šolta (43.42°N, 16.25°E). Measurements were made with these moorings from October 2005 through September 2006 (11 months) utilizing the trawl-resistant Barny Sentinel design (Perkins et al., 2000) for protection from the heavy fishing activity of this region. The DART in situ instrument deployment period spanned the period 23 Oct., 2005 to 23 Sep., 2006. It utilized mooring measurements, drifter data, towed Conductivity, Temperature and Depth (CTD) measurements, turbulence profile measurements, numerous standard CTD casts, remote sensing of temperature, optics, and roughness, high-resolution atmospheric and ocean models, and wave models to realize various research goals. It also included field experiments and cruises conducted in winter during 2–25 Mar. (DART06A) and in summer during 16 Aug.–23 Sep. (DART 06B). This work is focused mainly on the summertime results.

The main purpose of this work is to analyze the DART remote sensing and in situ observations, and numerical model results obtained from NCOM, to develop a kinematic description of the eddy variability and gain insights into the underlying dynamics, with an emphasis on the role played by the associated wind fields. Section 2 describes the remote sensing and in situ data, and the circulation model characteristics. Section 3 describes the observed eddy features. Section 4 presents the model predictions, and Section 5 closely examines filament development. Section 6 considers regional statistics. Section 7 investigates upwelling processes. Section 8 discusses the results. Section 9 summarizes the major conclusions and considers the significance of the work for Rapid Environmental Assessment, coastal monitoring and prediction.

2. Methods

2.1. Remote sensing data

Remote sensing imagery spanning the entire Adriatic Sea was acquired from the MODIS sensors on board the NASA Terra and Aqua satellites. The satellite orbits are sun-synchronous and the images are acquired daily at local equatorial crossing times of 10:30 a.m. (Terra, AM, descending mode) and 13:30 p.m. (Aqua, PM, ascending mode). The daily AM and PM images were processed to yield estimates of SST and Chl-a (obtained from the OC3M algorithm). The imagery acquired by NRL spanned the period 1 Feb. through 7 Nov. 2006, i.e. 2006 Julian Days-of-Year 2006 (henceforth JDays) 32–311, and thus overlapped most of the DART in situ instrument deployment period. The raw image sequences were posted to a secure DART project website in near-real time in a compressed, Joint Photographic Experts Group (JPEG) format during the winter and summer experiments to facilitate operational cruise planning. Complete image series for the full Adriatic and a zoom spanning the DART experimental domain were animated and the resulting movies were later posted to the project website. The image sequences were edited to remove those with excessive cloud cover, dropouts, or artifacts due to atmospheric water-vapor anomalies, based on a subjective judgement of the visible areas of interest and comparisons between corresponding SST and Chl-a images. The resulting image sequences were analyzed to identify particular events including the formation of eddies and filaments and their spatial and temporal evolution. Sample images from the movie sequences appear in the presentation posted on the REA conference web site (URL http://geos2.nurc.nato.int/mreaconf/ppt/5.8.pdf).

In the absence of strong estuarine inputs or evaporation/precipitation, sea surface salinity (SSS) tends to be a conservative tracer of freshwater influence; however, Chl-a concentrations, being biochemically active, must be regarded as non-conservative. Furthermore, obtaining accurate Chl-a concentration estimates from satellite optical sensors is challenging due to the need to model and remove atmospheric effects and infer the chemical concentrations from the observed optical properties, often in the presence of interfering factors such as high turbidity in shallow coastal (Case II) waters (Hu et al., 2000). Consequently, any comparisons between satellite-observed Chl-a and modeled or in situ SSS need to be interpreted with caution. As a physical variable subject to radiative (sensible) and evaporative (latent) heat fluxes, SST is also non-conservative. As a result of such fluxes, the thermal signal of freshwater plumes associated with land/sea temperature differences is rapidly reduced in intensity with time. Remotely sensed from space using infra-red radiometers, the measured SST also suffers from potential inaccuracies due to atmospheric water-vapor modeling and correction uncertainties. As a 'conservative' tracer SST thus tends to fall between Chl-a and SSS. Visual comparisons between MODIS Chl-a and SST imagery indicate clearly that these parameters tend to correlate well in winter. However, the Chl-a preserves significantly more information about estuarine inputs than does SST in the summer, when formation of the seasonal thermocline tends to obscure the underlying thermal structure. As mentioned by an anonymous reviewer and substantiated by Artegiani et al. (1997a,b), the wintertime water column is vertically well mixed and fresh, cold, nutrient-rich Po River water tends to be confined along the coast, while in the presence of summertime stratification, this water tends to spread seaward in a thin surface layer and experiences significant surface heating. Unfortunately, due to frequent and heavy cloud cover, there are relatively few useful images available covering the Adriatic Sea in winter. Those which exist for winter 2006 show that frontal boundaries associated with eddies and filaments tend to be well represented by both the Chl-a and SST fields. Structures apparent in the Chl-a fields tend to appear or disappear in response to chemical and biological processes, while those evident in SST are preserved by the underlying physical processes (water mass-exchange, advection, etc.) at more or less constant or slowly-varying levels. Thus, while we use Chl-a for detecting eddies and filaments and studying their shape and size evolution in this study because of its greater information content, we avoid making inferences based on changes in the Chl-a intensity (concentration) alone. We also focus on the summertime period during which more cloud-free images are available.

2.2. In situ data

Hydrographic transects were obtained using a ship-deployed AquaShuttle Mk III undulating towed vehicle developed by Chelsea Technologies Group Ltd of Surrey, UK. The vehicle was fitted with a Conductivity, Temperature and Depth measuring system with an associated fluorometer (Mini Pack CTD-F). The raw CTD data were processed using the manufacturer's software and calibration coefficients. The fluorometer data were calibrated using a relative scale, and are displayed in arbitrary units. The vehicle was towed at typical speeds of 4 m s^{-1} (8 knots) within a 3 to 5 m s^{-1} (6 to 10 knots) range. Pressure, temperature and conductivity data were sampled at a frequency of 10 Hz and the instrument was cycled over depths varying over the range ~5–30 m, depending upon the known depth of the bed and of the thermocline, which was the main feature of interest. Tows were typically conducted over periods of several hours and over distances spanning tens of km.

Due to the high and varying vehicle speeds and strong temperature and salinity gradients, salinity 'spiking' was significant. This artifact is associated with probe misalignment and temperature sensor lag relative to conductivity (Horne and Toole, 1980; Gregg and Hess, 1985) and the thermal inertia of the conductivity probe (Lueck, 1990; Lueck and Picklo,

1990; Morison et al., 1994). Spiking was minimized by applying a simple delay of 2.75 s to the temperature probe, before computing salinity from temperature and conductivity using the 'standard' algorithms (UNESCO, 1983). This delay was chosen as a compromise between minimizing the residual standard deviation and maintaining an acceptable signal to noise ratio (applying a lag tended to increase the C–T cross-correlation at low frequencies, but decrease it at high frequencies, thus generating noise in the S computation). The resulting S data were low-pass filtered with a 150-pt. box car filter to eliminate any residual spikes. The data were also smoothed with a 225-pt. Blackman low-pass filter, having an effective horizontal spatial cutoff scale of ~100 m, thus producing a despiked and smoothed data set suitable for contouring. Attempts to apply the Lueck (1990) model to correct for the thermal inertia of the conductivity probe were not successful due to the high and variable tow speeds and unknown variations in the 'angle of attack' of the sensors. The technique of matching up and down casts to define parameters for this algorithm (Morison et al., 1994) could not be employed because of differences in the apparent vertical profile for the up and down casts caused by the forward motion of the probe in the presence of large horizontal gradients as the instrument cycled through upward and downward excursions. Despite the lack of a suitable thermal inertia correction, remaining biases are likely small in comparison with the large in situ T and S variability associated with the WAC frontal structure and summertime stratification.

Measurements were made during the 11 month current meter deployment period with Barny ADCP moorings at sites along the GS line (Fig. 1). We focus here on data from moorings GS1–GS4, which spanned the WAC as it crossed the Palagruña Sill. In addition to current measurements obtained at 15-minute intervals throughout the water column (0.5–3.0 m depth cells excluding the surface and bottom interference zones), the moorings also recorded bottom pressure, temperature, and salinity. During the winter (Mar. 2006) and summer (Aug.–Sep.) experiments, additional moorings were deployed just downstream of Cape Gargano to capture the evolution of the frontal and eddy fields. A majority of these moorings were the newly-developed Shallow water Environmental Profiler in Trawl-resistant Real-time (SEPTR) configuration moorings. During DART, the SEPTRs used ADCPs to measure currents throughout the water column (0.5–1.0 m depth cells, excluding the surface and bottom interference zones) at 15-minute intervals and the retractable buoy to make CTD casts every 6 h. Here, we use data from SEPTR mooring sites B50, B75 and B90 and Barny mooring site A20 (Fig. 1). Only those DART instrument sites that were used in this work are shown in the figure.

2.3. Model description

The numerical hydrodynamic model predictions were made using an enhanced version of the Navy Coastal Ocean Model (NCOM, Martin, 2000; Martin et al., 2006, 2009). NCOM is a primitive equation, Boussinesq, vertically-hydrostatic model with an implicit treatment of the free surface and a generalized vertical grid (with upper layer sigma-coordinates and optional level coordinates below a specified depth). The model uses third order upwind advection and the Mellor-Yamada Level 2 vertical mixing scheme (see Martin et al., 2009 for other details).

Boundary parameters were specified using bathymetry, river inflows, and atmospheric forcing data. The bathymetry was derived from a Naval Oceanographic Office database and nautical chart soundings and the land/sea boundary was derived from the Generic Mapping Tools (GMT) vector shoreline. The model domain was tilted clockwise by a mean angle of 47° relative to true north (the model plots point upward towards the northwest).

River inflows were incorporated using a source term, and were simulated using climatalogical monthly inflows (Raicich, 1994) except for the dominant Po River, for which observed daily discharges were used. The Po discharge was spread over 5 discharge locations spanning the delta to simulate the river's actual distributaries. During the period Feb 1, 2006 to Oct 2, 2006, which spanned the DART experiment, observed and climatological mean Po River discharge rates were 744 and 1463 $m^3\ s^{-1}$, respectively. The observed Po R. discharges used to drive the model were slightly less than half the annual mean discharge of 1585 $m^3\ s^{-1}$.

Atmospheric forcing data were generated by the Croatian Meteorological and Hydrological Service using the ALADIN atmospheric model (Ivatek-ahdan and Tudor, 2004). The NCOM model was initialized at 00Z Jan. 1, 2005 using initial conditions for sea surface height, current velocity, temperature and salinity obtained from the NRL's global NCOM model (Barron et al., 2004). (See Martin et al., 2009 for other details of the Adriatic model's initial and boundary conditions.)

3. Eddy evolution

3.1. Isolated eddies

Examples of isolated mesoscale anti-cyclonic eddies formed on the downstream (i.e., southeast) side of Cape Gargano are apparent in the remote sensing images of JDays 32 (1Feb), 49 (18 Feb), 184–186 (3–5 Feb), 204–210 (23–29 Jul), 215–219 (3–7 Aug.), 245–250 (2–7 Sep), 259–265 (16–22 Sep) of 2006. Each interval coincides with a particular event, but does not necessarily span it fully because some of the adjoining images were clouded. The observed isolated eddies are typified by the one that was present on 5 Sep., 2006 (JDay 248, Fig. 2a). In the MODIS Chl-a image shown, a filament of higher-Chl-a water (>0.5 mg m^{-3}) projects eastward from the eastern tip of the cape and curves anti-cyclonically (clockwise) around a lower-Chl-a region. High-Chl-a waters also appear in the Gulf of Manfredonia south of the cape, where some smaller-scale frontal features also appear. The sequence shown in Fig. 3 indicates that this high-Chl-a filament first appeared at the tip of the cape on 2 Sep. It then translated and rotated clockwise and was well developed and starting to straighten out then recurve eastward by 6 Sep. It had largely disappeared by 11 Sep., which suggests an evolution time scale of 4–9 days. However, the appearance of some residual low Chl-a concentration features suggests that the anti-cyclonic eddy circulation responsible for the development of this filament persisted over a longer time scale. Also conditions appeared to revert to something resembling their initial state on 2 Sep., perhaps presaging the start of another eddy formation cycle.

While there were a few small meanders or cusp-like features northwest of the cape during this period, only one of these persisted and none showed any obvious signs of development, translation, or rotation. This pattern suggests that the larger eddy formed in isolation, near the tip of the cape. The smaller-scale features appearing immediately south of the cape, and along the coast to the east, on the other hand, showed some indications of rotation and translation or stretching toward the southeast. This and the anti-cyclonic rotation of the dominant stream suggest that the features were experiencing strong horizontal shear of the along-shelf WAC flow. Such shear would tend to favor rotation and growth, or at least stretching produced by shear dispersion, of any constituent features projecting from the coast.

3.2. Multiple eddies

Examples of multiple eddies forming west of and around the cape appeared on JDays 39 (8 Feb.), 89 (30 Mar.), 166 (15 Jun.), 175–178 (24–27 Jun.), 187 (6 Jul.), 199–203 (18–22 Jul.), 270–276 (27 Sep.–3 Oct.) and 289–291 (16–18 Oct.) of 2006. These eddies, which also show anti-cyclonic curvature, are typified by the one present on 2 Oct.,

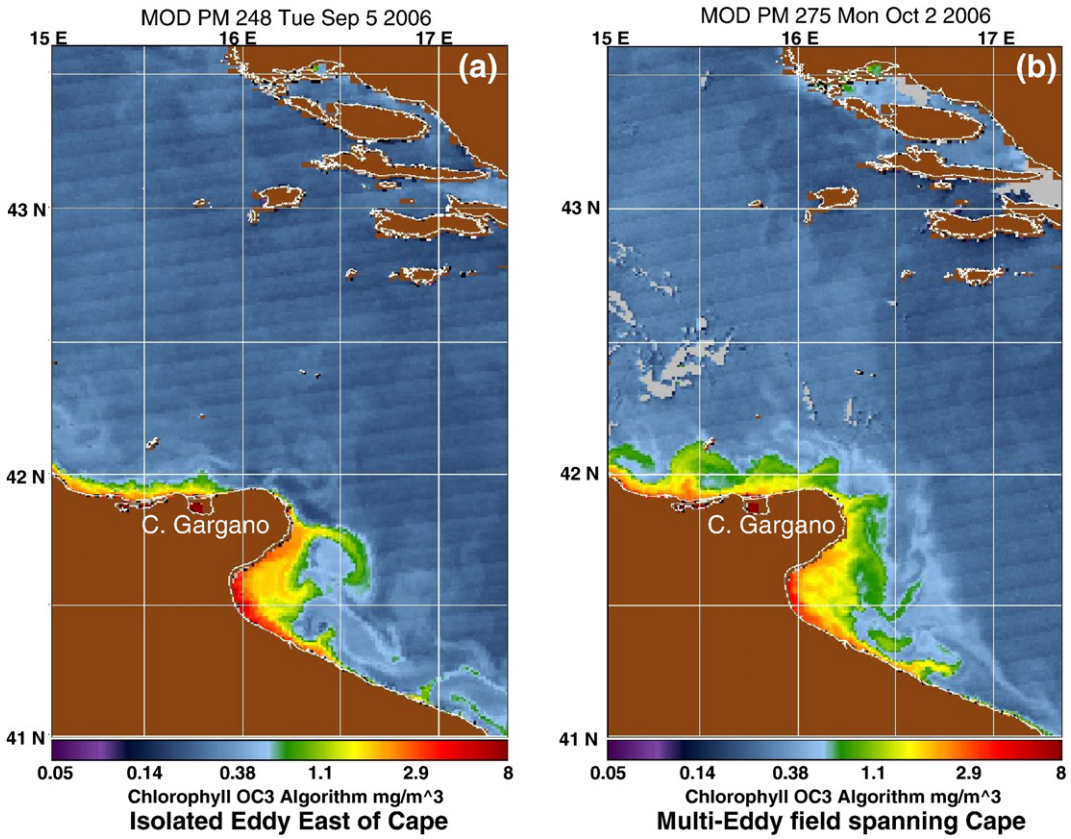

Fig. 2. Eddy development around Cape Gargano. (a) Single isolated eddy formed downstream of the cape on 5 Sep., 2006. (b) Multiple-eddy field formed in the vicinity of the cape on 2 Oct., 2006. The chlorophyll color axis labels (mg m^{-3}) are linearly distributed based on the natural logarithm of the values.

2006 (JDay 275, Fig. 2b). In the Chl-a image, a spatial sequence of at least four eddies appears upstream of the cape. Another is located at the tip and perhaps two less well-formed offshoots appear downstream of the cape, but with filaments that are not quite so well organized as in the isolated-eddy case discussed above. The multiple-eddy features are spread along the shelf with a longitudinal separation scale that indicates an effective crest-to-crest 'wavelength' of 28–37 km. These wavelengths are similar to those estimated by Korotenko (30–35 km) for features for the TM, which typically appears about 100 km upstream. The wavelengths of those TM meanders exceeded their estimated internal deformation radius, R, by a factor of 2.6. The agreement with linear stability theory predictions led Korotenko to assert that they were generated by baroclinic instabilities, an explanation that likely also applies to the features we observe near the cape.

The MODIS image sequence shown in Fig. 4, which duplicates the image of Fig. 2b in Fig. 4e, indicates that the features evident in Fig. 2b had undergone significant prior changes. They began with formation on or before 27 Sep. when they were fairly regular bulges (Fig. 4a). They developed filaments with initially anti-cyclonic (4a) then cyclonic (4b–d) curvature immediately north of the cape and showed evidence of downstream translation over the succeeding 3 days. By 2 Oct. (Fig. 4e) there were 7 distinct, well-organized eddy features tending towards anti-cyclonic circulation, at least close to shore. These had weakened the following day (Fig. 4f). This sequence suggests two possible interpretations: Either changes in wind or boundary current strength are generating alternately cyclonic or anti-cyclonic across-shelf current shear over time, or a meandering, quasi-steady mid-shelf jet (the WAC) is shedding eddies in space that tend to be cyclonic off shore and anti-cyclonic near shore. Some combination of these two processes might also be occurring. To discover whether these interpretations might apply more generally, we examined the other multiple-eddy event sequences that occurred during JDay ranges: 175–178 (24–27 Jun.), 199–203 (18–22 Jul.), and 289–291 (16–18 Oct.). We found variants of the patterns hypothesized above to be commonly observed. Of these, the first event sequence showed evidence of cyclonic filament curvature north and west of the cape, with an anti-cyclone to the east. The second event sequence showed features similar to those of JDay range 270–276 (27 Sep.–3 Oct., Fig. 4), but the JDay 200 PM and 201 AM, PM (19–20 Jul.) images additionally showed eddies forming a vortex 'street' southeast of the tip of the cape. The third event sequence again showed cyclonic eddies to the north and west, and an anti-cyclone to the east of the cape. Several individual instances of multiple eddies on specific JDays (unfortunately with the adjoining image sequence obscured by cloud) showed this tendency, with occasional formation of a 'mushroom' jet projecting east from the cape, formed from a cyclonic eddy to the north paired with an anti-cyclonic eddy to the south.

Due to the large number of images that were obscured by cloud, the above evidence must be regarded as potentially biased toward particular patterns. A more systematic search for such sequences is possible using model predictions (Section 4) and their statistics (Section 6), but first we consider the possible role played by fluctuations in the along-shelf wind and associated changes in the direction and strength of the WAC in the observed eddy sequences.

3.3. Wind influence

The evolution of eddies and filaments discussed above suggests the dominant effect of time-varying along-shelf advection and across-shelf shear associated with the WAC. We now examine both unfiltered and low-pass filtered wind and current data for the period JDay 186–210 (5–29 Jul, Fig. 5). In this figure and in the remainder of this paper we adopt the oceanographic directional convention for winds, so that a wind blowing from the southeast (e.g., during a Sirocco event)

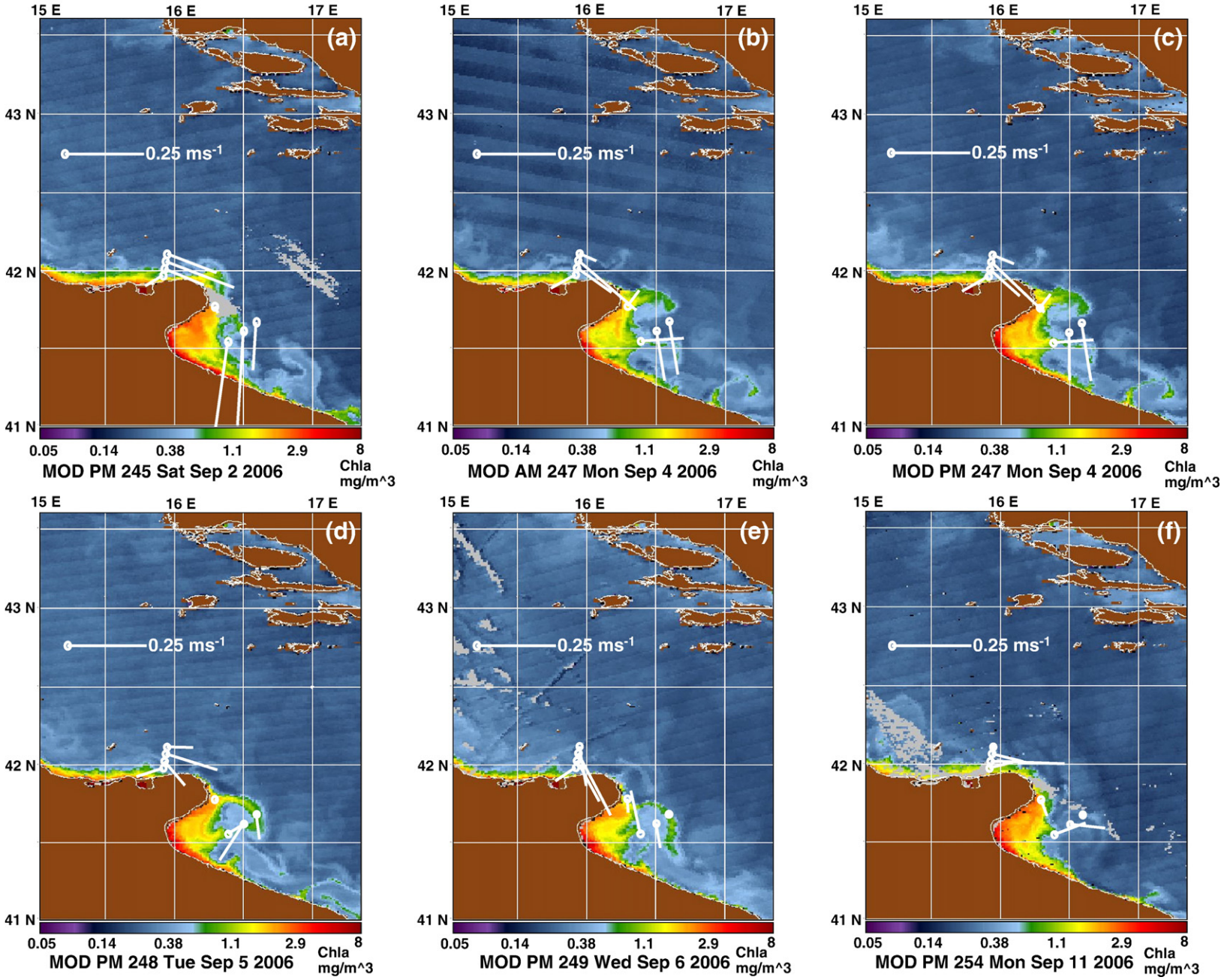

Fig. 3. Evolution of a single isolated-eddy sequence over (a)–(e) 2–6 Sept, 2006 (JDays 245 PM, 247 AM–PM, 248 PM, 249 AM) and (f) on 11 Sep., 2006 (254 PM). Current velocity vectors at the current meter mooring locations are superimposed. These vectors are from data depth-averaged over 5–15 m, and low-pass filtered with a 25-h cutoff period. The directions are relative to north (up) and the magnitude scale is 0.25 m s^{-1} per half degree of latitude (e.g., velocity at GS3 in (a) is 0.25 m s^{-1}).

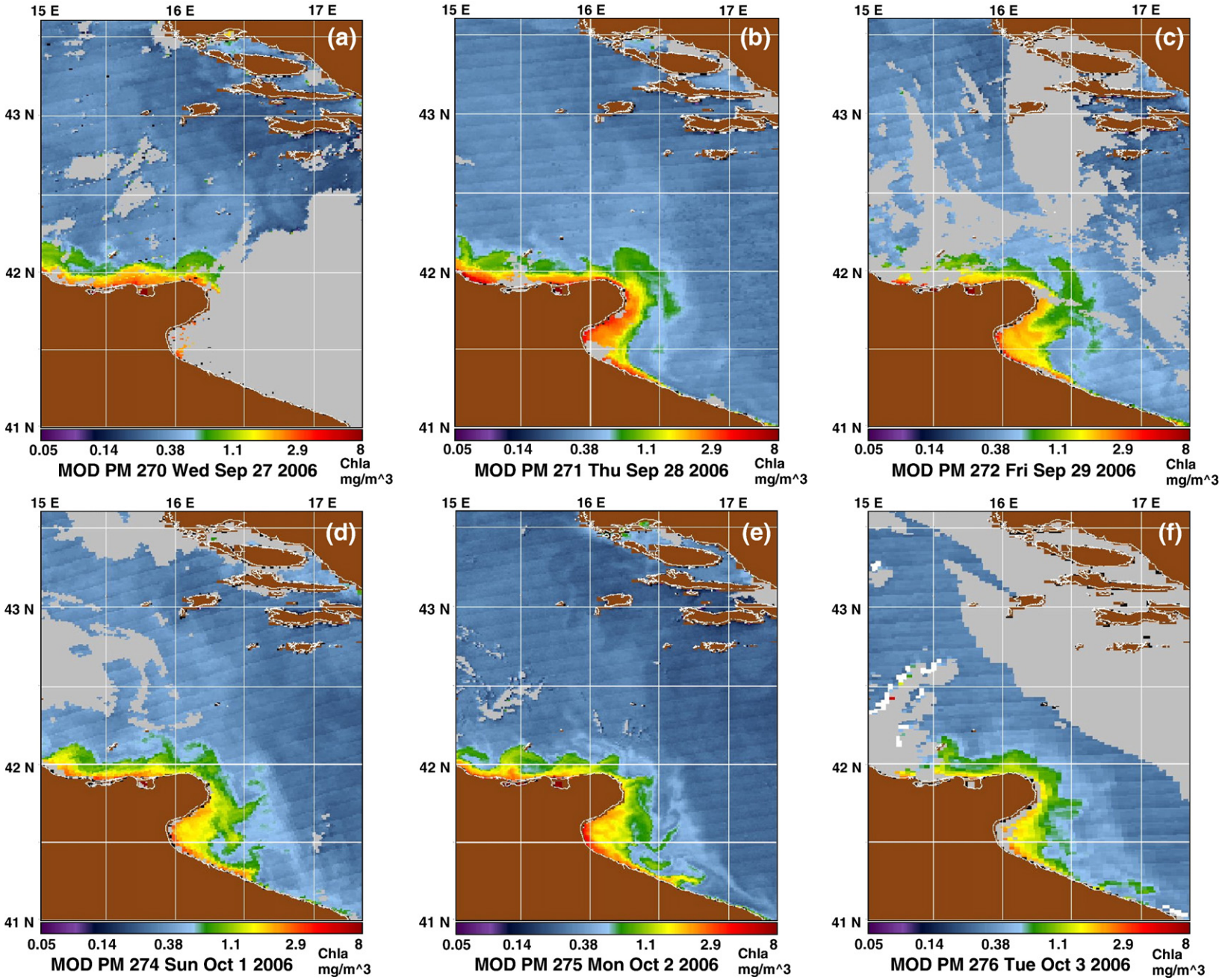

Fig. 4. Evolution of a multiple-eddy sequence over (a)–(c) 27–29 Sep., 2006 (JDays 270–272 PM) and 1–3 Oct. 2006 (274–276 PM). Current moorings were not deployed during this period.

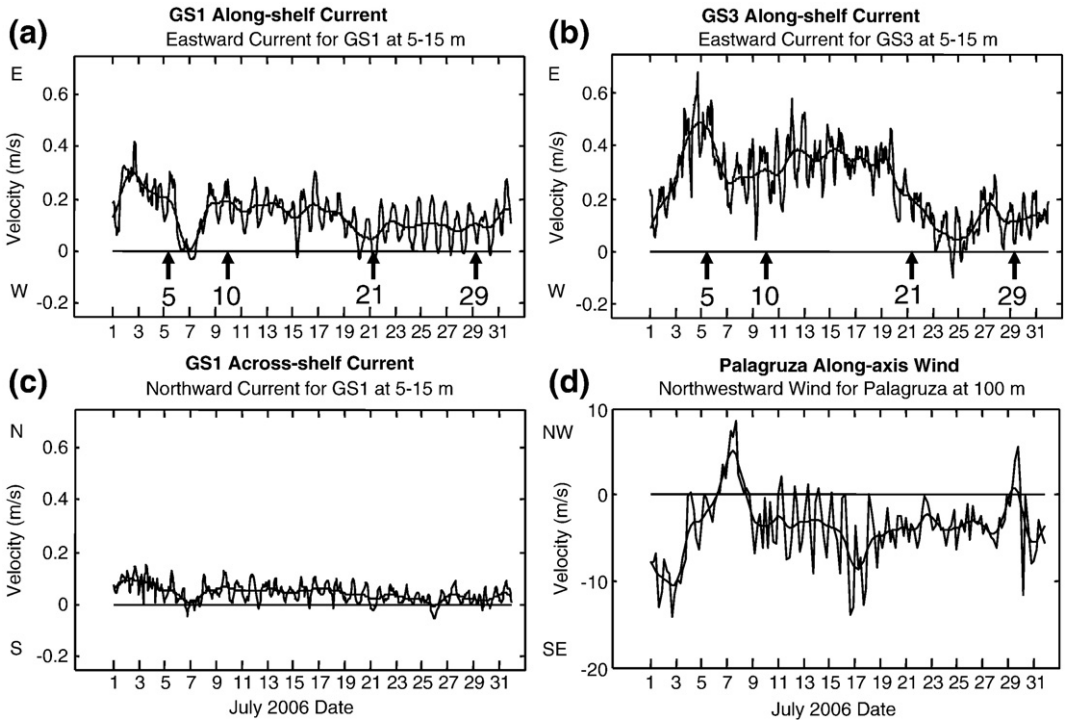

Fig. 5. Currents and winds for July (spanning MODIS images in Fig. 6). Eastward (along-shelf) current at (a) GS1 and (b) GS3, (c) northward current (across-shelf) at GS1 and (d) corresponding northwestward wind velocity component at Palagruza Island. Instantaneous sample values are plotted with 25-h cutoff period low-pass values (smooth solid line) superimposed.

would be described as blowing northwestward. The filter used was a 51-h long Hamming filter, with a cutoff period of 25 h intended to remove tidal and sea-breeze influences. During this period, both isolated and multiple-eddy events occurred (current data are not available for the sequence JDay 270–276 (27 Sep.–3 Oct) that appears in Fig. 4). Currents measured at the inshore (GS1) and mid-continental shelf (GS3) locations immediately west of Cape Gargano (Fig. 5a–c) during Jul., 2006 show fluctuations in current direction and magnitude that are associated with changes in wind strength and direction at Palagruza Island in the central Adriatic (Fig. 5d). Prevailing low-frequency currents during July were almost exclusively eastward, locally along-shelf, with a weak, almost reversed, flow event occurring in the first half of the month at GS1 (during 6–7 Jul., after strong eastward flows that exceeded 0.5 m s^{-1} at GS3). Two similar events occurred in the second half, during which the eastward currents were generally weaker. According to Cushman-Roisin et al. (2001, p. 94 and references cited therein), northwestward wind events can cause the flow along the Italian coast and even the entire WAC to reverse direction, but while the low-frequency currents stalled they did not reverse at GS01 or GS03 in early July 2006. At GS1, across-shelf currents were weak, presumably due to the coastal constraint. At GS3 (not shown), across-shelf currents showed greater high-frequency variability, but no obvious low-period signal. Similarly, the across-axis winds at Palagruza (not shown) were relatively weak.

Winds offshore during July blew predominantly southeastward, favoring downwelling along the Italian coast. These winds were strong during the first week and for a few days mid-month and during the last week. Both the Palagruza weather station (PWS) wind and GS3 current were more energetic during the first half of the month than during the second, and with the exception of trends during the first week they appear visually to be weakly anti-correlated. This is to be expected as local northwestward (southeastward) wind stress will tend to oppose (reinforce) an eastward current. While southeastward wind stress was strong (but diminishing) in the first week, the eastward currents became progressively stronger. As the winds reversed direction to northwestward, the current velocities decreased. The currents strengthened slightly during mid-month as the downwelling-favorable southeastward winds increased. Both winds and currents then relaxed so that a period of relative calm followed with reduced high-frequency variability, punctuated only by a brief but strong northwestward (upwelling favorable) wind event in the last week. There are some similarities between the GS1 and GS3 current patterns, but the relationship with the wind is less apparent for GS1, which is closer to shore, where the wind is likely influenced by the topography of the elevated land associated with the cape (Pasari et al., 2007, 2009-this issue). Spatial variability in the winds evident in the analyzed wind products (Section 4) might also explain apparent differences in the timing of the first wind relaxation event and the current response. It is also known that during some strong wind events (e.g., bora) the WAC is forced by remote rather than local winds (Book et al., 2005; Martin et al., 2009).

The appearance of eddies and filaments during July appears consistent with the wind and current data. The initial downwelling-favorable, southeastward winds suppressed eddy activity (6 Jul., Fig. 6a). As these relaxed and then became upwelling favorable, a multiple-eddy sequence formed (10 Jul., Fig. 6b). This situation reverted to a weak downwelling-favorable condition in the second half of the month (21 Jul., Fig. 6c) when winds were calmer and the eastward current was relatively weak. Finally, a large anti-cyclonic eddy and associated offshore jet evolved east of the cape (from 21–29 Jul., Fig. 6c, d). This jet might have been derived from the eastward filament flow projecting from the cape on 21 Jul. While there was no evidence of an associated current response at GS3, the offshore expansion of this feature coincided with the brief upwelling-favorable wind event that occurred during the last week of July.

4. Model predictions

After a preliminary startup period, the NCOM hydrodynamic model was run from 1 Nov., 2005 to 27 Sept., 2006, a period which spanned the DART winter and summer field campaigns. Here we present representative fields of predicted SSS for comparison with the MODIS Chl-a imagery.

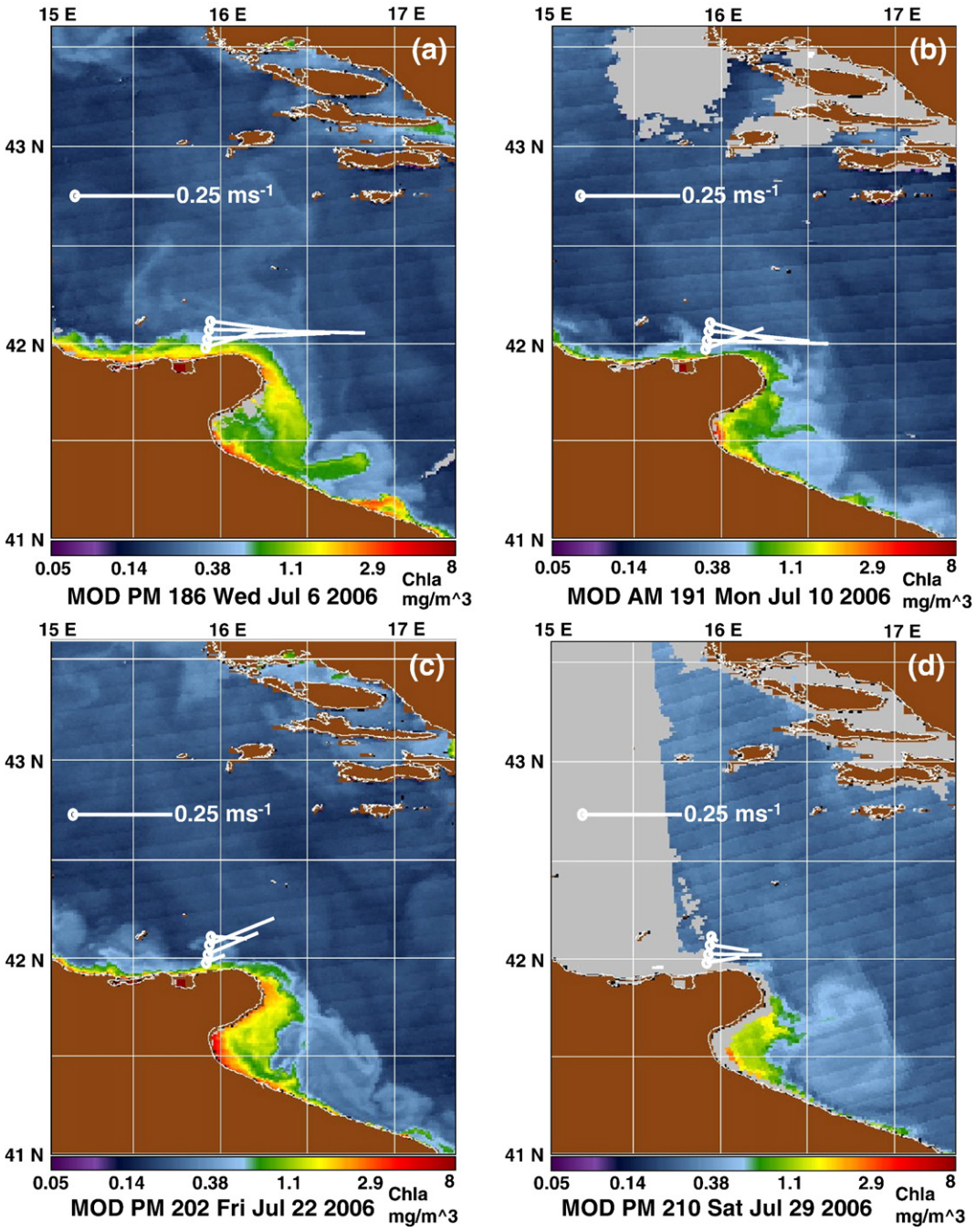

Fig. 6. Chl-a images corresponding to the times marked (by arrows) in Fig. 5 (a) 5 July (JDay 186 PM), (b) 10 July (191 PM), (c) 21 July (202 PM) and (d) 29 July (210 PM). Current velocity vectors at current meter mooring locations GS1–4 are superimposed (A20 and B50, 75, 90 were not deployed). These vectors are from data depth-averaged over 5–15 m, and low-pass filtered with a 25 h cutoff period. The directions are relative to north (up) and the magnitude scale is 0.25 m s^{-1} per half degree of latitude.

4.1. Surface hydrographic fields

Model simulation frames portraying SSS, currents and winds were extracted from the simulation files, assembled in time sequence and studied for correlations among these parameters. We first present a sequence corresponding to the formation of an isolated eddy in the Gulf of Manfredonia, followed by a multiple-eddy sequence, both corresponding to available remote sensing imagery.

4.1.1. Isolated-eddy sequence

The model SSS field on 2 Sep. 2006 (Fig. 7a) shows downwelling-favorable southeastward winds blowing at approximately 5 m s^{-1} along the central axis of the Adriatic Sea and parallel to the Italian coast (the model grid is oriented approximately northwest–southeast). Winds immediately east of the cape are weaker than elsewhere, perhaps due to the sheltering effect of the cape's elevated topography (Pasari et al., 2009-this issue), but they remain strong offshore. The WAC flows strongly eastward, paralleling the coast with evidence of only weak meanders, but it separates as it rounds the cape, and there is anti-cyclonic circulation in the lee of the cape. By 4 Sep. (Fig. 7b), the winds have relaxed, and the meanders are larger in amplitude. The anti-cyclone in the lee of the cape forms a double-cell structure and the circulation is intensified and closed, forming an eddy. On 5 Sep. (Fig. 7c), southeastward winds are reestablished and they persist, but weaken slightly, the next day. There is little apparent change in the circulation on 6 Sep., however, an animated sequence

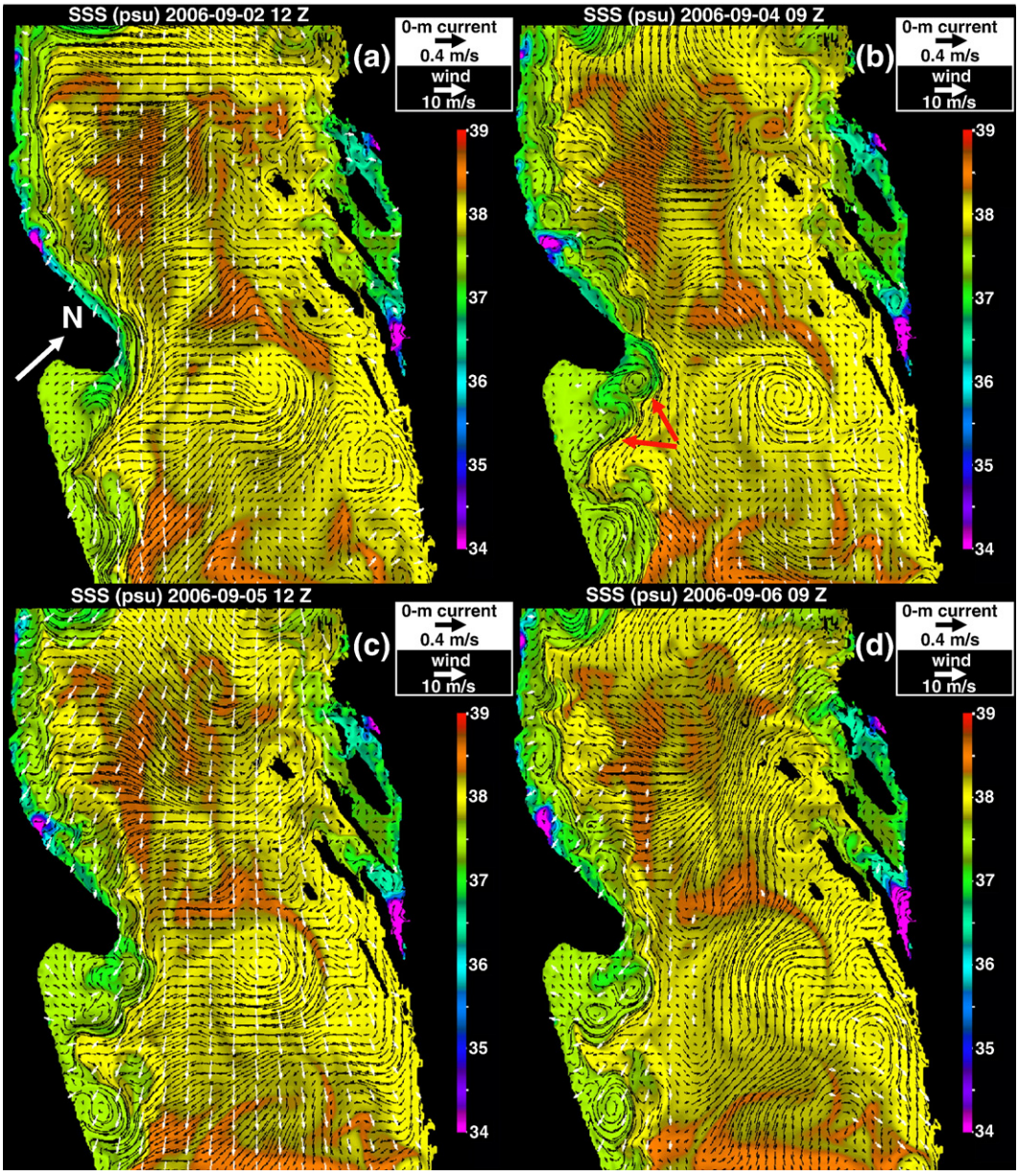

Fig. 7. NCOM predicted SSS field of isolated-eddy case for (a)–(d) 2, 4–6 Sep., 2006. These may be compared qualitatively with the MODIS imagery presented in Fig. 3. White and black arrows are wind and current vectors, respectively, while the salinity color scale ranges over 34–39 psu, from magenta to red. Winds weaker than 2 m s^{-1} are not plotted. The white arrow in (a) indicates true north, and the red arrows in (b) mark eddies resembling those aligned along section A in Fig. 9a.

of model frames (URL http://geos2.nurc.nato.int/mreaconf/ppt/5.8.pdf) clearly shows that there was progressive anti-cyclonic rotation and downstream translation of the eddy features during the 5-day period just described. Modeled surface currents in the central Adriatic during this period showed quite dramatic changes in magnitude and direction. These changes resulted in variations in the source area and intensity of flows feeding the WAC, but otherwise seemed to have little impact on the character of its flow along the Italian shelf.

Comparison with the Chl-a imagery on corresponding days (Fig. 3a–e) shows a consistent pattern with eddies and meanders largely suppressed upstream of the cape and only weak meander development throughout the period, while winds were strongly downwelling favorable. The progressive anti-cyclonic rotation and translation of the eddies and filaments downstream of the cape and formation of a double-cell eddy structure that are evident in the model animated sequence also agree with the remote sensing observations. This is highlighted by the development of the high-Chl-a concentration filament projecting eastward from the tip of the cape and curving anti-cyclonically into the Gulf of Manfredonia. This filament was sampled during the summer field campaign and its in situ horizontal and vertical structures are described in Section 5.

4.1.2. Multiple-eddy sequence

Model frames corresponding to the sequence of eddies and filaments evident in the Chl-a imagery during Jul. (Fig. 6) are presented in Fig. 8. To aid interpretation, some additional frames for dates lacking corresponding cloud-free remote sensing imagery are also included. The model frame of 5 Jul. (Fig. 8a) shows weak downwelling-favorable winds (white arrows) blowing southeastward and shoreward along the Italian coast. The wind tends to curl anti-cyclonically around Cape Gargano, perhaps due to the previously mentioned topographic effect. This could reinforce any tendency for anti-cyclonic ocean circulation in this area. The WAC is evident as an intense stream flowing eastward along the shelf (black arrows). The

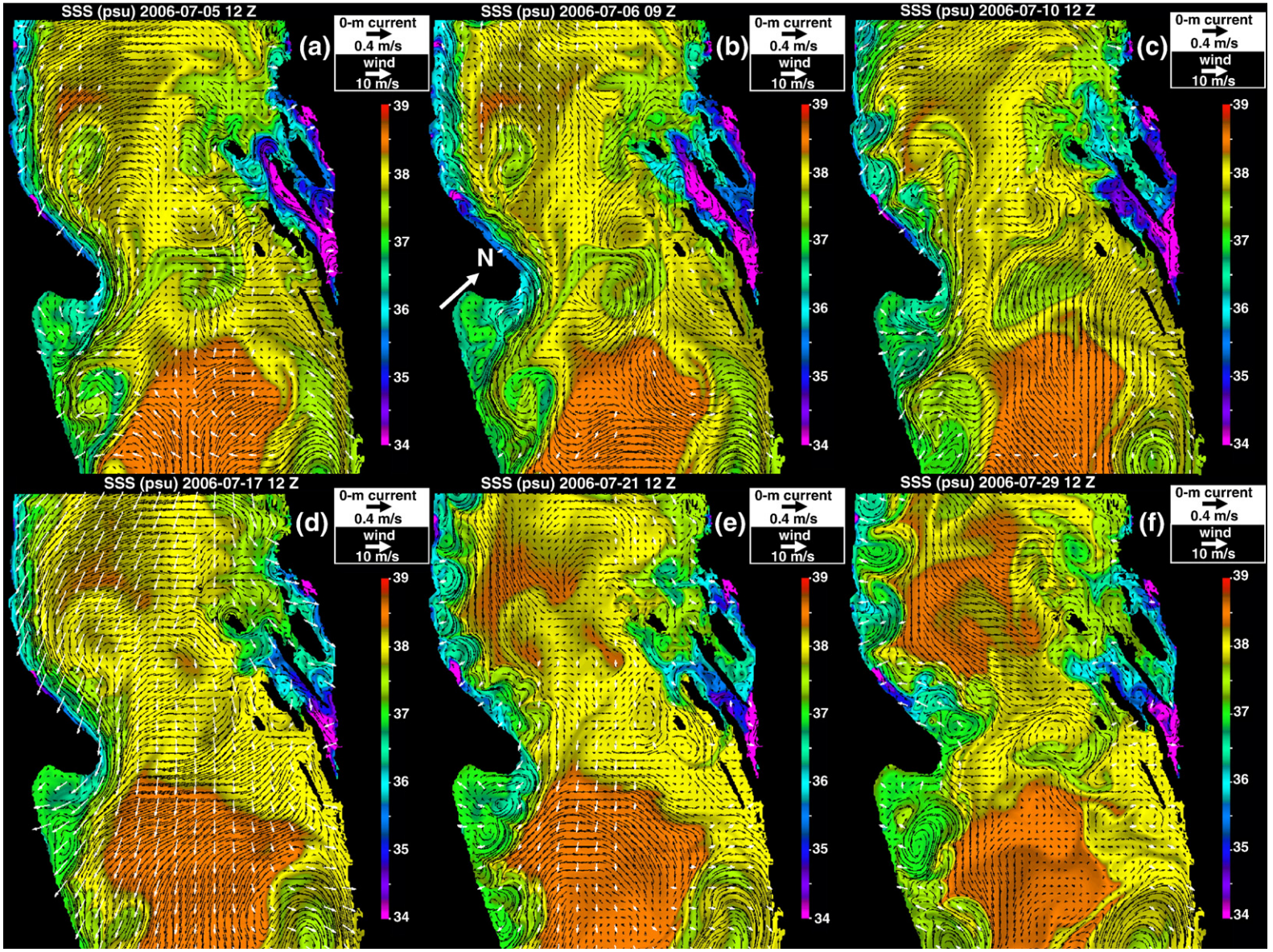

Fig. 8. NCOM predicted SSS field for multiple-eddy case for (a)–(f) 5, 6, 10, 17, 21, and 29 Jul., 2006. Those of 5, 10, 21 and 29 Jul., may be compared qualitatively with the MODIS imagery presented in Fig. 6. The white arrow and color scales are as described in the caption to Fig. 7.

flow parallels the coast, upstream of the cape, but separates as it rounds the cape and crosses the Gulf of Manfredonia. After rounding the cape, it tends to produce a westward branch, which forms an anti-cyclonic 'lee' eddy near the cape, and an eastward branch, which forms a matching cyclonic eddy further downstream. In some frames, there is evidence of confluence of the WAC flow with the Rim Current which flows around the northern boundary of the SAP. The point of separation of the resulting combined flow and its subsequent point of impingement on the coast vary from frame to frame. The lee eddy resembles one described by Kleypas and Burrage (1994) and Burrage et al. (1996) in the East Australian Current as it rounds the southeast tip of the Great Barrier Reef (see Section 6 discussion). There is also evidence of a large filament extending from the coastal impingement point into the central Adriatic. The filament's appearance does not seem consistent with the prevailing flows, so it may be a residual feature, from a previous offshore filament. A similar filament was shown to cross the Adriatic eastward in model results described by Vilibić et al. (2009-this issue). A similar but smaller feature, which appears in our model results north of Cape Gargano, may be related to the northward jet modeled by Korotenko, 2007.

The next day's model frame (Fig. 8b) shows calm winds near the cape and the WAC front shows some evidence of meandering further upstream. This may be a response to the relaxation of the winds on 6 Jul. By 10 Jul. (Fig. 8c), after they had become briefly upwelling favorable then relaxed to weakly downwelling, the meanders intensified and three anti-cyclonic boundary current eddies formed upstream.

On 17 Jul. (Fig. 8d), winds were again strong and downwelling favorable, and the meanders and eddies were strongly attenuated. Meanwhile, the dipole eddy structure located east of the cape at the start of the sequence persisted. By 21 Jul. (Fig. 8e), the downwelling winds had relaxed and a multiple-eddy structure had formed, exhibiting an unbroken sequence of eddies or meanders along the visible length of the WAC, including an eddy triple-cell structure east of the cape. On 22 Jul. (not shown) the eddies and meanders grew in offshore extent and there is a sign of the anti-cyclonic eddies coalescing and intensifying east of the cape. By 29 Jul., winds had reversed direction, there was strong offshore flow east of the cape, weak cyclonic and anti-cyclonic features closer inshore, and a larger anti-cyclonic circulation cell located a little further downstream (Fig. 8f). The model simulation thus follows a complete cycle with the winds alternating twice from down through upwelling favorable and the WAC responding with alternately suppressed or expressed multiple-eddy structures, while anti-cyclonic flow persisted east of the cape.

Comparison with corresponding images of Chl-a (Fig. 6), shows general agreement but the cycle is incomplete (e.g., there is no image for 17 Jul.), and either less intense, or not so clearly expressed. The image of 5 Jul. (Fig. 6a) shows clear signatures of the modeled downwelling response with little evidence of meandering or eddy formation except for the anti-cyclonic eddy east of the cape. The images of 10 and 21 Jul. (Fig. 6b, c), on the other hand, show multiple-eddy development, consistent with the character of the circulation, if not the flow details, found in the simulation. The image of 29 Jul. (Fig. 6d) shows a large anti-cyclonic feature east of the cape, consistent with the model predictions. Well-developed eddies appearing west of the cape in the simulation are not obviously present in the Chl-a image, which, however, is largely obscured by cloud in that area.

Examination of the entire simulation record shows that alternating cycles of downwelling- and upwelling-favorable winds are associated with strong modulation of the mesoscale eddy fields, suggesting that winds are a key factor governing the intensity of mesoscale variability in the Adriatic. The patterns found in the remote sensing imagery tend to reinforce this relationship, but the evidence must be regarded as circumstantial, given the limited database of cloud-free image sequences spanning such up- and downwelling wind cycles.

5. Filament development

We now examine the development and 3D structure of the isolated eddies and filaments described in Section 3.1. The horizontal structure of these features is well illustrated by the Chl-a image of 4 Sep. AM, which appears in Fig. 3b and is reproduced in Fig. 9a. The image shows what appears to be a double-cell structure with a pair of anti-cyclonic eddies appearing north and south of the 41.5° latitude line to the east of the cape with high-Chl-a filaments wrapping around their northern rims. The low-pass filtered near-surface velocity vectors from the Barny ADCPs at stations A20 and B50–90 (see Fig. 1 for locations) are shown superimposed on each of the images. Southward low-frequency flow is evident at the eastern tip of the main filament at B90 and B75 until 6 Sep when the flow weakens and then becomes eastward. The flow is due east on 4 Sep. at B50, which lies in the path of a secondary filament separating the northern and southern anti-cyclonic eddies (comprising the previously mentioned double-celled feature). At A20 the flow is northeastward, and the Chl-a image suggests that it is feeding the flow in the main filament mentioned above. It later shifts to the southeast (Fig. 3e, f) and by 11 Sep. appears to be feeding the secondary filament at B50.

Data acquired from the Aquashuttle show a vertical section through the northern anti-cyclonic eddy (Fig. 9b–d), following a south to south–southeast trending transect (dashed line, A in Fig. 9a). The fluorescence section (F in Fig. 9b) shows evidence of Chl-a concentrations peaking at a depth of 20 m with an apparent signal (exceeding background levels) spreading about 10 km horizontally and penetrating to a depth of at least 27 m. The region shallower than 17 m was not sampled, but presumably the signal at this depth is continuous with the remotely-sensed surface signal (Fig. 9a). The salinity signal (Fig. 9c) shows a horizontal frontal structure with a strong salinity gradient located near the southeastern side of the Chl-a filament separating higher salinities to the southeast from lower salinities to the northwest in the upper layer. A relative minimum on the fresh side of the front also occurs, roughly corresponding to the location of the Chl-a peak. There is an undulating, but apparently continuous, zone of intermediate salinity values (38.2–28.3 psu) spanning the entire section; a similar, but less obvious zone appears in F. It is apparent from the temperature section (Fig. 9d) that this zone approximately follows the seasonal thermocline, suggesting that fresher, higher Chl-a concentration water has been mixed into this zone. The greater vertical extent of this zone of relatively fresh, higher Chl water (Fig. 9b, c) at the extreme southeast of the transect may indicate the presence of the secondary filament that appears east of B50 in the Chl-a map (Fig. 9a). The intermediate body of more saline and lower Chl-a concentration waters occupying the upper layer in the southeast portion of the transect (at distance 22 km and depth 20 m) could represent deep-ocean water intruding southward along the rim of the northern anti-cyclonic eddy (near B90, Fig. 9a). The doming of T at the location of the filament (Fig. 9d) could be a manifestation of entrainment of deeper cooler water into the high-Chl-a 'jet', or of upwelling associated with streamline curvature as discussed in Section 8. It could also be a consequence of the dynamics of the double-cell circulation structure (T strongly dominates S in its effect on the density field in this region). If subject to bottom friction or wind stress, an anti-cyclone (which exhibits high central pressure) may experience Ekman pumping (Wolanski et al., 1996; Takahashi et al., 2007; Mahadevan, et al. 2008). This generates downwelling at its center and upwelling around its rim, which, based on the remote sensing image (Fig. 9a), is skirted by the filament. However, there is no corresponding doming of isohalines, and S is higher beneath the feature, which seems to preclude vertical entrainment or upwelling as an explanation for the doming of T. Horizontal entrainment of cooler water at depth was also considered. The corresponding Modis SST image (not shown) indicates that there is warmer water at the surface ~26 °C that is only a half degree cooler near the coast; a temperature

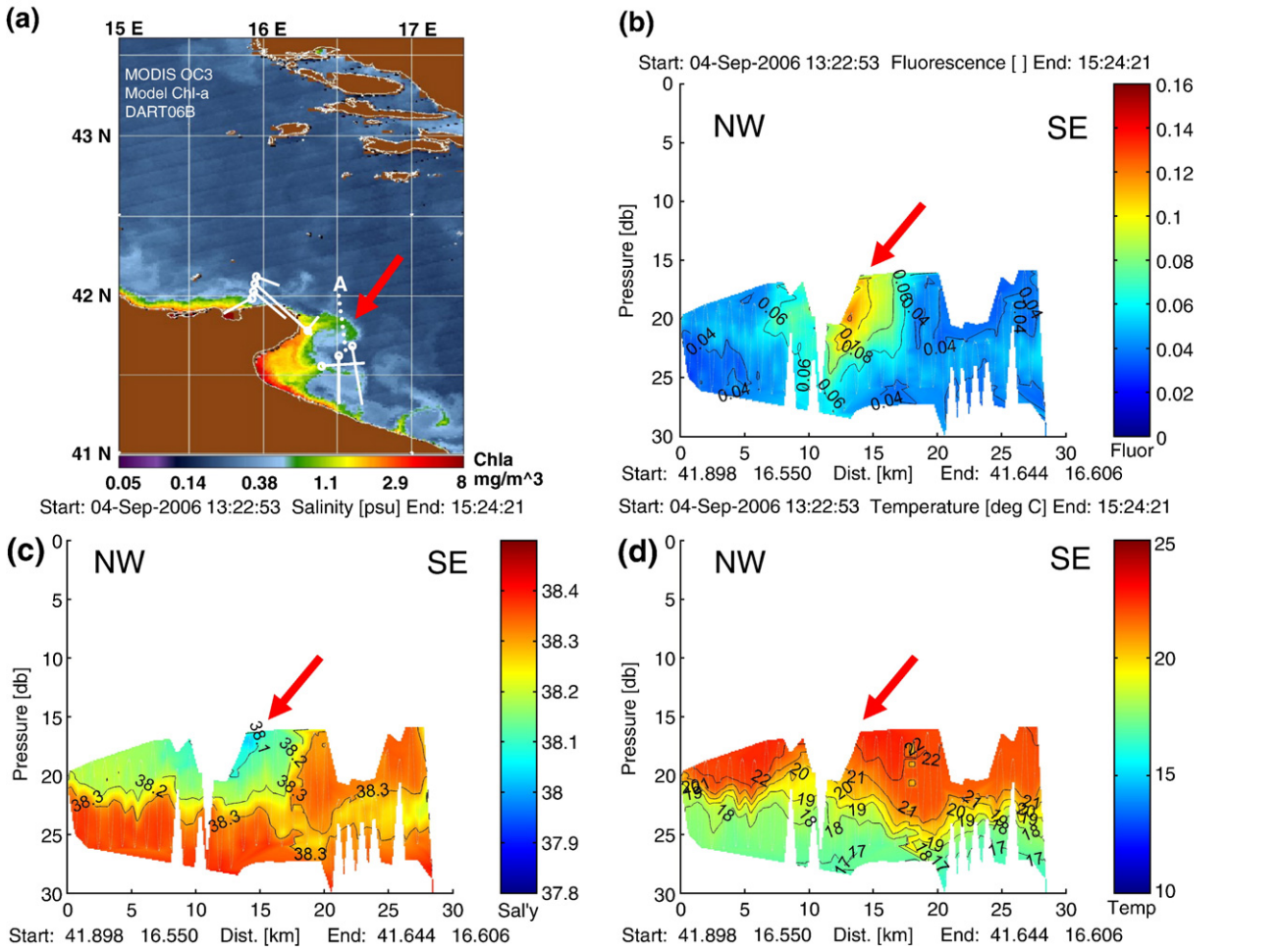

Fig. 9. a) MODIS Chl-a image on 4 Sep., 2006 (JDay 247 PM) (repeated from Fig. 3c) with mean velocity vectors (solid lines) originating at the mooring locations (open circles) overlaid. The dashed line indicates the Aquashuttle transect. (b)–(d) Aquashuttle vertical sections along the transect of fluorescence, salinity and temperature, respectively. The high-Chl-a filament, characterized by high F, low S and high T appears in the vertical sections and coincides with the surface filament in the satellite image (see red arrows).

difference that is insufficient to account for the domed feature, which exhibits horizontal temperature differences of 2–3 °C.

An indication of the temporal evolution of the eddy field can be gleaned from the time series of current velocities that span the remote sensing sequence (Fig. 10). Vertically-averaged currents in the upper layer in the depth range 5–22 m (Fig. 10a) show strong southeastward flows at B50–B90 sometimes exceeding 40 cm s^{-1} alternating with periods of weaker or reversed flows of 20 cm s^{-1} or less. Flows are generally weaker at A20 and rotated from northward on 4 Sep. to southward on 6 Sep. Station B90 flow was predominantly southward, while B50 showed mostly eastward flows, and B75 was mostly southward during the same interval, consistent with the 'snapshot' of 4 Sep. (Fig. 9a) and indicating an Eulerian time scale (with features persisting in place over a period) of about 4 days. However, the Chl-a image sequence 2–11 Sep. (Fig. 3a–f), shows that the features persist much longer, with Lagrangian time scales of at least 10 days and perhaps several weeks, as they are rotated and advected downstream in the mean WAC flow. The vertically-averaged currents at B50–B90 in the lower layer depth range of 22–45 m (Fig. 10b) are similar in direction, but much weaker in magnitude, consistent with the existence of density stratification and indicating that the velocity structure is mainly baroclinic.

An appreciation of the horizontal spatial scale of these features can be gained directly from their size in the MODIS images, which show the two eddies downstream of the cape with diameters of order 18 and 28 km. The vertical S section obtained from the Aquashuttle data (Fig. 9c) along transect A in Fig. 9a does not fully span the northern eddy but gives a lower bound of 15 km, while the model (Fig. 7b) predicts a pair of similar looking features, displaced in location, with diameters of 17 and 25 km. The vertical (depth) scales are of order 22 m in the Aquashuttle data and about 13 and 23 m in the model. The MODIS Chl-a signal associated with the filament indicates a width of about 7 km for that feature. The Aquashuttle (Fig. 9c) shows the filament to be about 8 km wide and 25 m deep.

Currents at the mooring locations appear consistent with the motion of the eddies and filament in the remote sensing image sequence (Figs. 9a and 3). Some indication of likely circulation patterns to fill in this picture can be obtained from the model predictions (Figs. 7b and 11a–f). Two sets of vertical sections of model S, U and V fields are shown in Fig. 11. U represents the current vector component tangential to (flowing along) the section, while V represents the component normal to (flowing across) the section. The vertical sections follow transects A1 and A2, which parallel the actual Aquashuttle transect A (Fig. 9c), but are displaced progressively to its west at intervals of 4 km and aligned closely with the predicted eddy locations (Fig. 11d–f). The model does not show eddies along the actual Aquashuttle transect. The model S field (Fig. 11a) is similar in character to the observed Aquashuttle S transect (Fig. 9c), although we do not expect close correspondence due to model sensitivity to small changes in initial or boundary conditions, and the inherent instabilities of both the predicted and observed flows. There is a salinity front in the model, on the northwest side of the northern

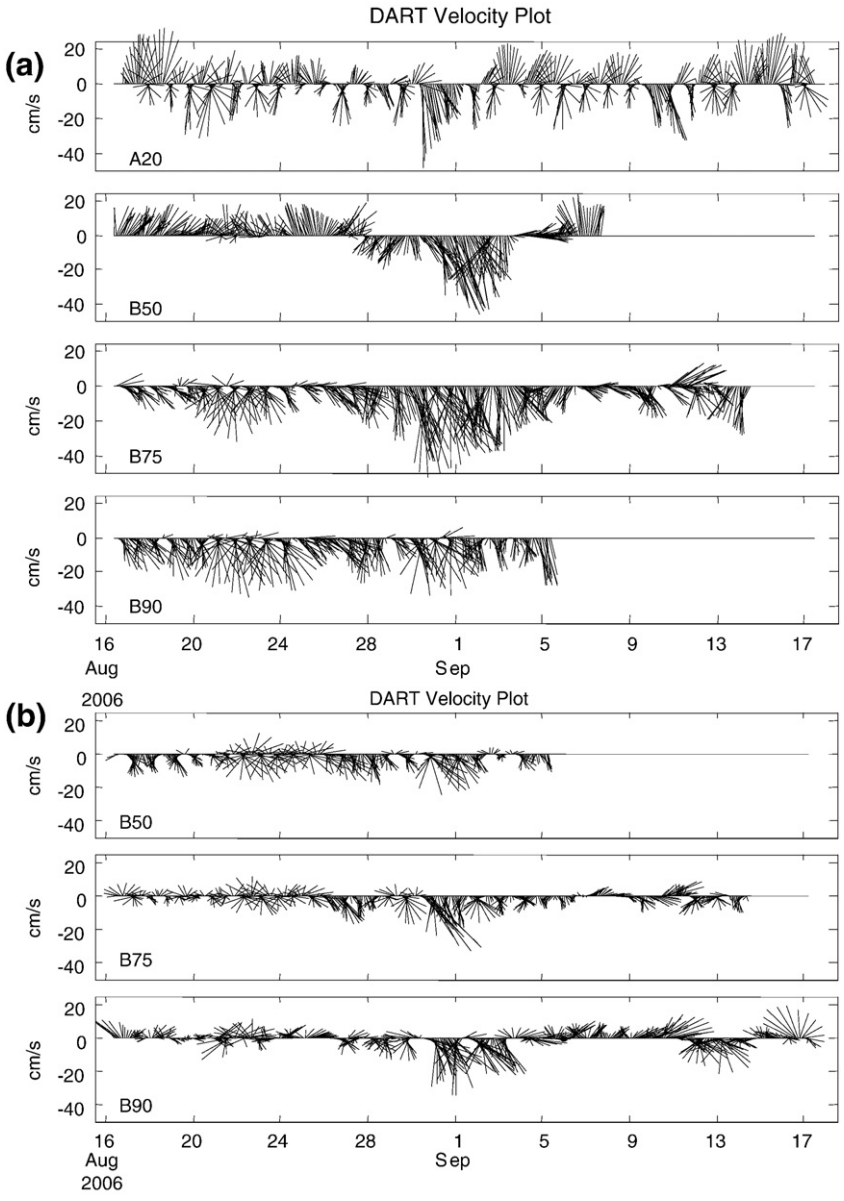

Fig. 10. Vector stick diagram for currents at moorings A20, B50–90 relative to magnetic north (up-direction). Currents were vector-averaged over depth ranges a) 5–15 m and b) 15–45 m during the period 17Aug.–17 Sep., 2006. Data were sampled at 0.25 h intervals, filtered with a 2.5 h cutoff dealiasing filter and sub-sampled to intervals of 1.25 h. Tidal signals thus remain in the record.

eddy, but the Aquashuttle section apparently did not extend far enough to the north to reveal such a feature. The eddy structure is clearly visible in the S and U sections, which are remarkably similar in appearance, while the anti-cyclonic circulation is evident in the changes of sign of the V component. Strong eastward flows exceeding 25 cm s^{-1} are evident on the northern rims of the eddies, while the return flows along the southern rims exceed 10 cm s^{-1}. This difference in intensity is evident in the surface velocity predictions on both 4 and 5 Sep. (Fig. 7b, c) and manifests itself in the MODIS image as strong and persistent entrainment of both the primary and secondary Chl-a filaments (Fig. 3b–e).

6. Regional statistics

The apparent similarities between features observed in the remote sensing imagery and those evident in the model suggest that the model predictions can be used to describe the general character and intensity of the central Adriatic circulation. We studied mean statistics based on the model predictions for all months spanning the model operational period of Nov. 2005 to Sep. 2006 and for the entire period. Here we present and compare mean statistics based on the model predictions obtained for the months of Jan. and Jul., 2006. These were found to be representative of statistics for the other months in the 2006 winter and summer seasons. The mean of the vector winds that was used to force the model in Jan. (i.e., in winter, Fig. 12a) blew towards the west over the central and northeastern side of the Adriatic, but veered to the south closer to the Italian east coast, forming a general bora pattern (Pasari et al., 2009-this issue). In Jul. (summer, Fig. 12b), mean winds blew with reduced intensity and mainly to the south, but with a southwestward component off the south-central Croatian coast. The sheltering effect of Cape Gargano is evident in both vector fields in reduced intensity and anti-cyclonic veering, but most obviously in July. The resulting shear could potentially influence across-shelf variations in the intensity of the WAC and may contribute to anti-cyclonic vorticity in the lee of the peninsula. The corresponding mean wind-stress curl fields (Fig. 12c, d)

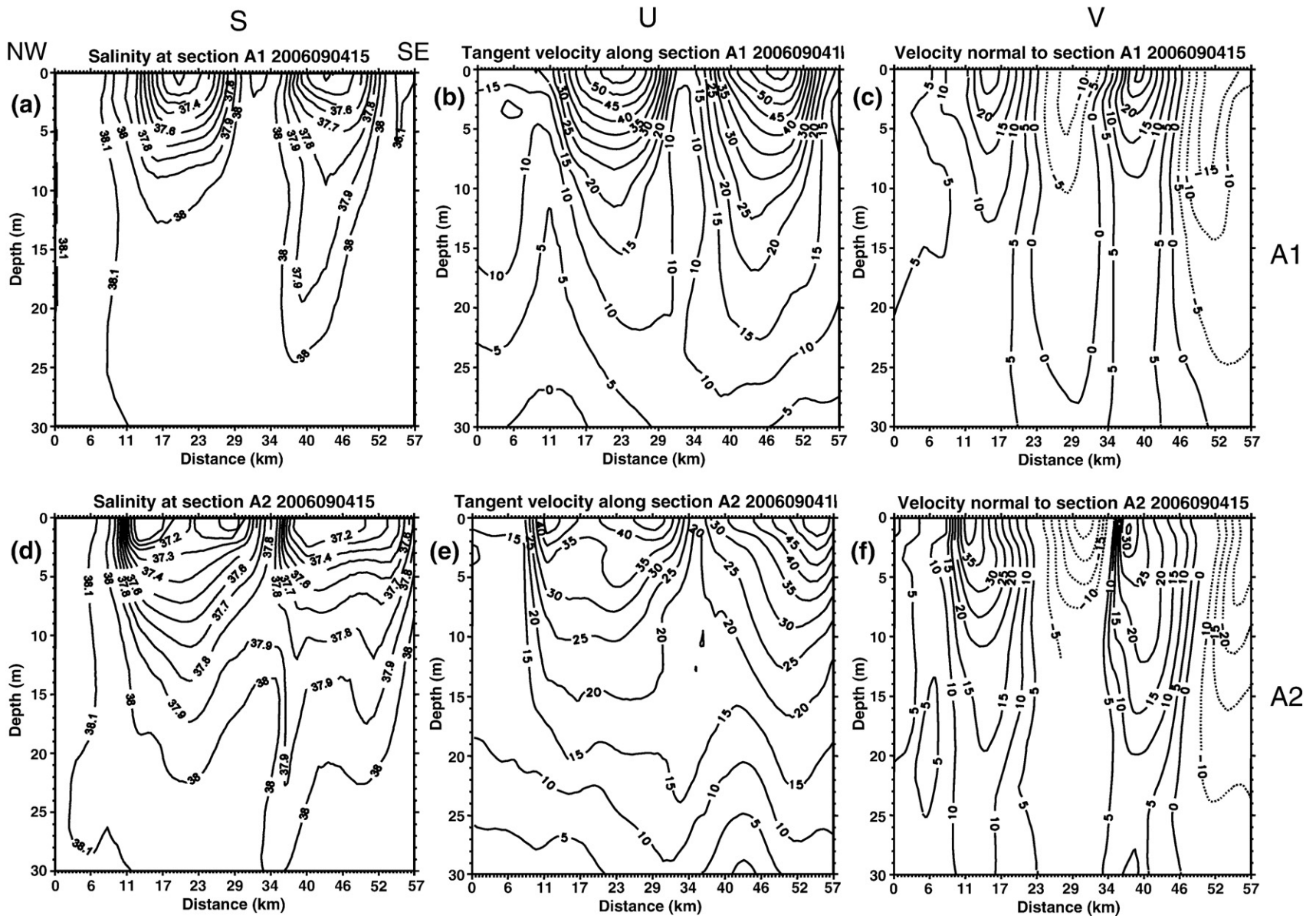

Fig. 11. Vertical sections from the NCOM model of (a, d) salinity, (b, e) tangential velocity and (c, f) normal velocity predicted along (top panels) sections A1 (located 4 km west of transect A in Fig. 9a) and (bottom panels) A2 (located 4 km further west of A1), respectively. Two anti-cyclonic circulation cells are clearly evident in the velocity sections and continuity of the structure between the two sections is apparent. Model section A (not shown), which coincided with the Aquashuttle section of Fig. 9, showed no apparent eddy structure, which indicates the predicted eddies lay further west than those observed in the MODIS and Aquashuttle data.

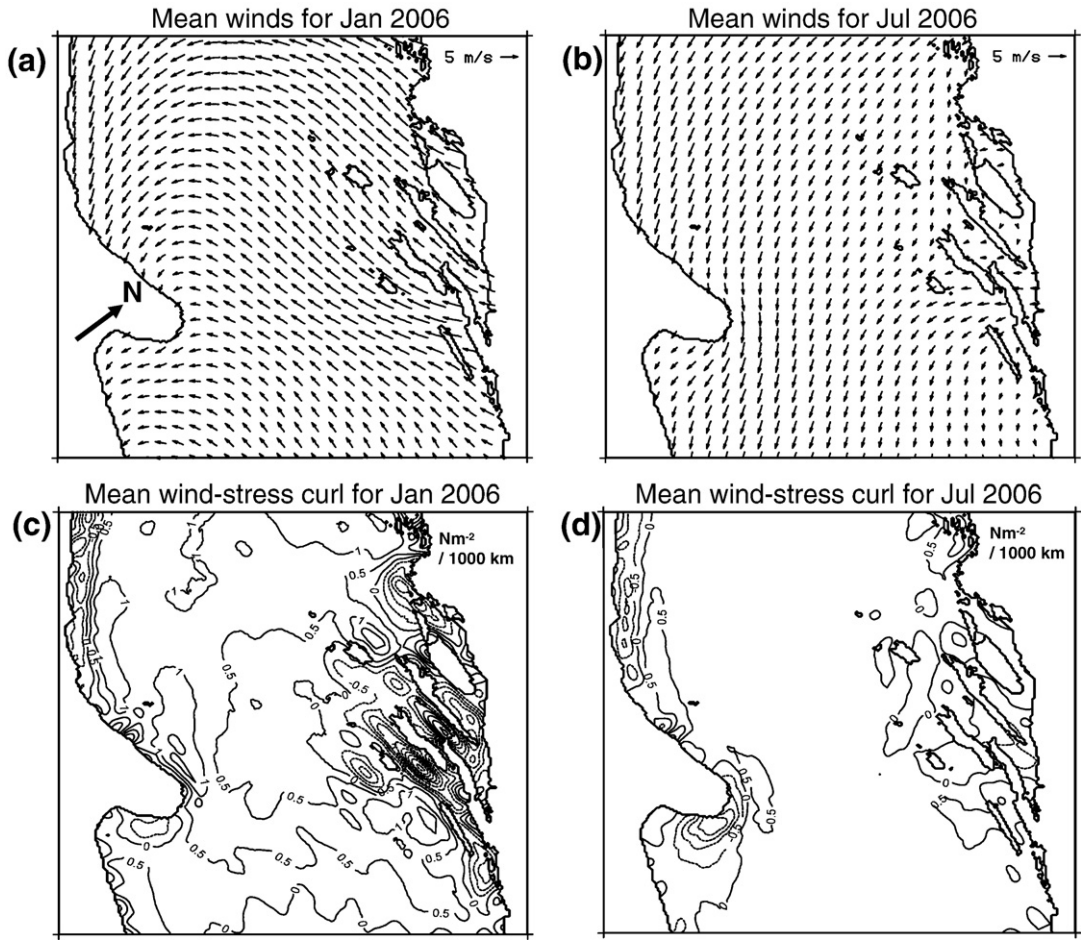

Fig. 12. Monthly-averaged mean winds (a, b) and wind-stress curl (c, d) for Jan (a, c) and July (b, d) 2006 in the central Adriatic region from the ALADIN model used to drive the NCOM model.

reinforce this interpretation by revealing a region of negative curl in the lee of the cape. A separate zone of negative curl also appears along the north-central Italian coast, while the curl is weak (particularly in summer), or positive, elsewhere.

The monthly Eddy Kinetic Energy (EKE) was computed as half the mean square of the deviations of the surface current from its monthly mean at each upper model grid cell, i.e., half the current variance with respect to the monthly mean. The Mean Kinetic Energy (MKE), was computed as half the square of the time-averaged flow. Both EKE and MKE are expressed in units of variance ($cm^2\ s^{-2}$). The pattern of EKE (Fig. 13a, b) broadly follows that of the Mean Kinetic Energy (MKE, not shown), which tracks the major Adriatic Sea currents, and it is consistent with the EKE found from analyzed drifter tracks (Poulain, 2001, his Fig. 4d). The pattern shows enhanced eddy activity along the Italian coast and close to shore, particularly in the north-central zone and around Cape Gargano. In the summer, the region of highest EKE (exceeding 500 $cm^2\ s^{-2}$), appears east of Cape Gargano and spans the Gulf of Manfredonia,(Fig. 13b). In winter, the high EKE region is confined near the tip of the cape and reduced in intensity, but is still the maximum (~500 $cm^2\ s^{-2}$) over the experimental domain (Fig. 13a). This band of high EKE follows the mean path of the WAC and the intensity is reduced as the shelf shoals south of the cape. It reduces rapidly to background levels of about 150 $cm^2\ s^{-2}$ seaward, but there is a broad feature of moderate intensity (about 300 $cm^2\ s^{-2}$) offshore of the main peak, near the southeast edge of Fig. 13b in summer. The relative vorticity computed from the model mean velocity field (Fig. 13c, d) shows broadly similar trends, but during winter it exhibits greater intensity west of the cape than it does to the east (Fig. 13c). This is likely a consequence of the high horizontal shear experienced along the WAC outer boundary, which is effectively trapped along a straight coast. Once it rounds the cape the intensity is reduced (Fig. 14c); perhaps as a consequence of the diverging isobaths. In summer, the vorticity is reduced to the west and intensified somewhat to the east relative to winter; the intensity differences on either side of the cape are largely equalized (Fig. 13d), perhaps because stratification isolates the stream from the divergent bottom contours. There is now a double maximum in anti-cyclonic (negative) relative vorticity east of the cape and in the Gulf of Manfredonia, with a small cyclonic (positive) feature inside the Gulf and located slightly to the west. Relative vorticity levels in the central Adriatic exhibit 'background' intensity levels of about $1\times10^{-5}\ s^{-1}$ ($\sim 0.1f$, where f is the Coriolis parameter) in both seasons, being slightly higher overall, and more variable in the winter. Unlike EKE levels off the Croatian coast, which are relatively weak, there are zones of high relative vorticity in this region (comparable with the Italian coast) in both seasons. Furthermore, there is evidence of island wake dipole eddy features present off both coasts, most readily seen on the Italian side, around the Tremiti Islands group northwest of Cape Gargano.

The model statistics shown are consistent with the observed high intensity of mesoscale eddy activity associated with the WAC in the vicinity of Cape Gargano. This feature appears comparable in intensity to the more closely studied zone of high eddy activity that appears along the north-central Italian coast (Poulain, 2001; Korotenko, 2007). The monthly mean fields suggest that these could be permanent

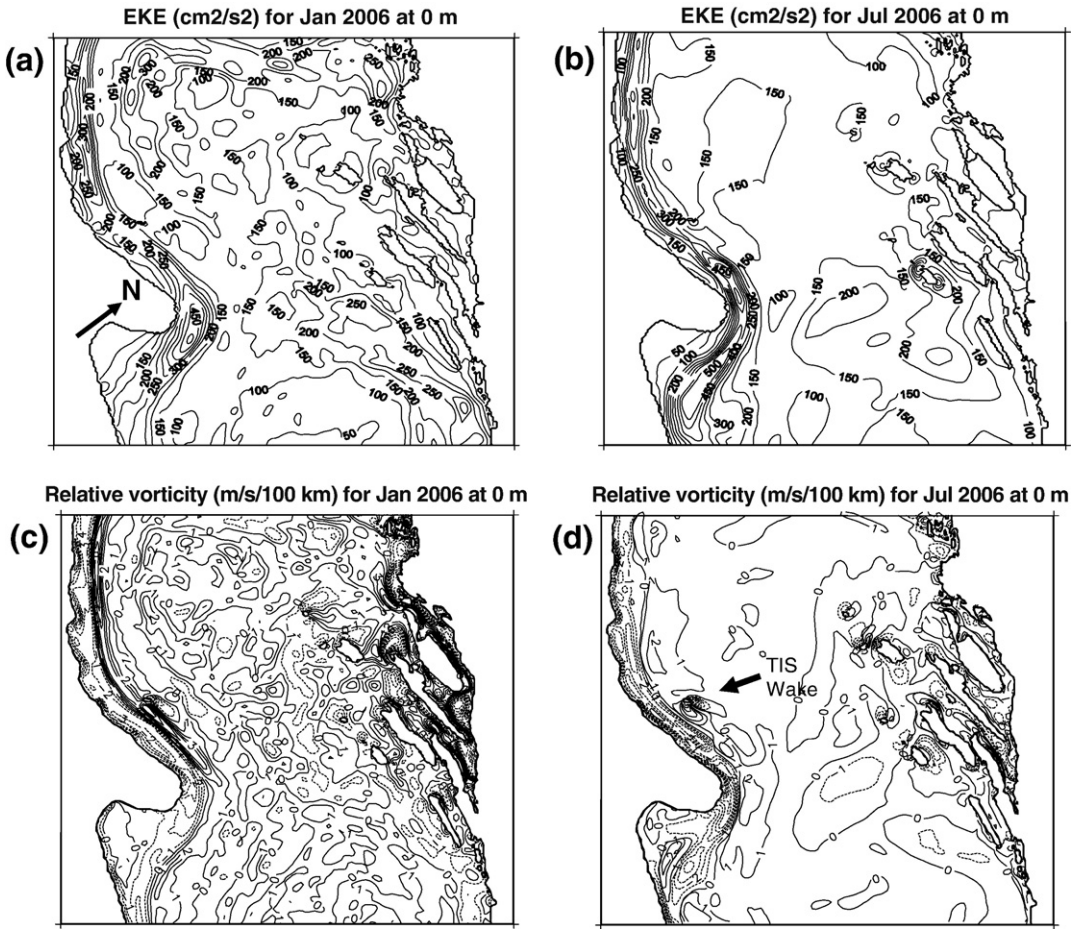

Fig. 13. Monthly-averaged NCOM model predictions in the central Adriatic region of Eddy Kinetic Energy (a, b) and relative vorticity (c, d) for Jan and Jul, 2006.

features which are intensified in the summertime stratified season, in spite of there being higher shear along the WAC boundary in winter.

7. Upwelling processes

Inspection of the monthly-averaged vertical velocity field of the NCOM model shows a patch of upwelled water at a point 5 km north of the 20 m isobath, which occurs off the cape in most of the modeled summer and winter months (e.g., June, 2006, Fig. 14a, solid white arrow). The upwelling velocity in this patch is about 2 m day^{-1} or 2.3×10^{-5} m s^{-1}. An across-shelf model vertical section parallel to and east of the GS mooring line (Fig. 14b) shows the same patch, marked by the solid white arrow in Fig. 14a, extending through the water column over the depth range 5–45 m. This upwelling patch appears in each of the 11 monthly-averaged plots during the DART experimental period (Nov, 2005 to Sept., 2006) with small changes in size and position across-shelf. It is not always present on a daily time scale, though, because it appears in the 2-day average vertical plot of 1–3 Sept., 2006, but is missing or much reduced in the subsequent 3–5 Sept. average (Fig. 14c, d). A plot of model bathymetry near Cape Gargano (not shown), indicates that the depth contours rounding the cape turn more sharply further to seaward than they do near the coast, effectively forming a ridge with an altitude above the ambient sloping bed of about 5 m and a point of minimum isobath turn radius appearing immediately downstream of the larger patch. An additional upwelling patch that has no surface manifestation appears further seaward over a depth range of about 45–115 m near the 20 km point (Fig. 14b). Bathymetry plots show that it appears above a 5 m high 'knoll' perched on the slope. The other monthly-averaged plots (not shown) indicate that this feature is confined to the lower half of the water column in summer, and is significantly reduced in July, but reaches almost to the surface in winter, suggesting that it is constrained by the seasonal stratification. In contrast, the inshore patch described above extends throughout the water column in all model months. Similar topographically-generated upwelling/downwelling patches reach the surface throughout the experimental domain, except in deeper water during summer, when they are confined to the lower water column. A notable feature of the upwelling velocity section (Fig. 14b) is the occurrence of relatively large and deep upwelling and downwelling features in the central Adriatic. These features might be driven in part by strong currents associated with the Palagruzza Sill crossing the steep topography, but since they are associated with the large-scale circulation, they are outside the scope of the present work.

A band of upwelling patches, which are not tied to bathymetric features, appears along the outer shelf west of the cape throughout the year, mirrored by a band of downwelling patches of similar size along the inner shelf. The 2-day averaged model vertical velocities show that upwelling and downwelling occurring on daily time scales in multiple-eddy fields could explain the appearance of a band of upwelling/downwelling along the outer/inner shelf in the modeled monthly-averaged vertical velocity fields. These upwelling and downwelling bands apparently exist in the statistical sense, as the integrated effect of transient upwelling and downwelling events occurring on the seaward and shoreward rims, respectively, of individual eddies as they rotate and translate along the shelf. The bands tend to follow the coastline west of the cape but depart from it, due to flow separation, as the WAC main stream and associated eddies round the cape toward the east. Unlike the persistent topographically-generated patches located east of the GS line, these patches are

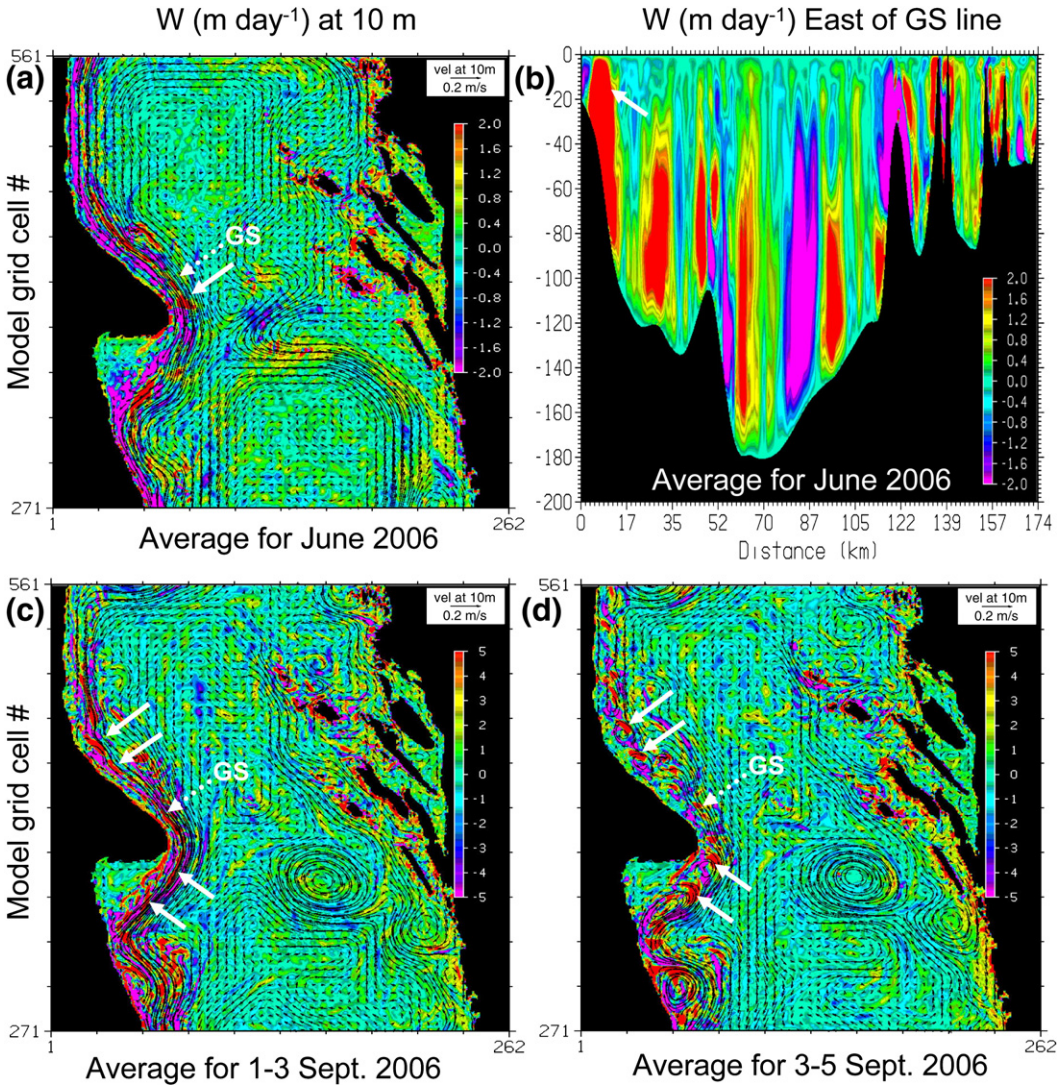

Fig. 14. Upwelling velocity predicted by NCOM model. Monthly-averaged vertical velocity during June, 2006 at (a) 10 m depth and (b) along a vertical section (solid white arrow) east of and paralleling the GS line (dotted arrow). 2-day averaged vertical velocity for (c) 1–3 Sept. and (d) 3–5 Sept., 2006. The solid white arrows denote a quasi-permanent upwelling patch appearing immediately south of the GS line in (a) and pairs of upwelling and downwelling features associated with transient mesoscale eddies in (c) and (d).

relatively shallow and vary in location, but their effect is to produce frequent upwelling along the outer WAC and downwelling along the inner WAC.

The most remarkable feature of the 2-day average plots for the smaller-scale circulation is the occurrence of pairs of upwelling and downwelling patches (marked by solid white arrows) on either side of the mesoscale eddies that appear both west and east of the cape. These patches exhibit vertical velocities of about $+/-5$ m day^{-1} or $+/-5.8\times10^{-5}$ m s^{-1}. The upwelling patches are located seaward and upstream of the downwelling patches on the rim of each eddy, but an animated sequence of 2-day averaged vertical velocity plots shows that the patches are stretched by the WAC current shear and propagate with the eddies as they advect eastward. Plots of model vertical velocity on vertical sections through these patches, show they are confined mostly to the upper layer (in summer), but may extend throughout more than half of the water column and they span the seasonal thermocline (e.g., ranging over 30 m in water 50 m deep, east of the cape). While the appearance of persistent upwelling may be explained by relative vorticity changes associated with curvature of the WAC stream as it rounds the cape or by flow interaction with specific bathymetric features (see Section 8), the origin of the upwelling and downwelling patches appearing on the eddy rims is unknown and requires further investigation. Existing theories of upwelling associated with mesoscale eddies based on secondary circulation induced by differential surface wind stress, across-stream shear or distortion of the eddy's circular shape, perhaps due to interaction with the bed, or non-linear dynamics may be relevant (Mahadevan et al., 2008 and references cited therein). Whatever their cause, the upwelling/downwelling patches along the seaward outer/inner rims of the mesoscale eddies in the 2-day vertical velocity plots could help explain the occurrence (on average) of zones of upwelling and downwelling that parallel the coast, and follow the outer and inner shelf, respectively, to the west of the cape, as found in the modeled monthly-averaged vertical velocity plots. Whether such features may be observable in reality is a topic for future investigation.

8. Discussion

Considering the apparent dominating influence of Cape Gargano and its associated coastal topography and bathymetry on the wind and current patterns in its vicinity; it is instructive to consider the role it plays in the absolute vorticity balance of the WAC circulation. Numerous authors (e.g., Arthur, 1965; Blanton et al., 1981; Kleypas and Burrage, 1994; Denniss et al., 1995; Pacheco et al., 2001; Doglioli et al., 2004; Munday and Marshall, 2005) have described the effects of coastal outlines and bathymetry associated with capes on the

Table 1
Vorticity and upwelling velocity dimensional estimates (see Arthur, 1965 for details of parameter specification and use).

	Value	Remark
a) Input parameter (unit)		
Latitude (°)	42	Approximate latitude of the cape
Coriolis parameter, f (s^{-1})	9.73×10^{-5}	Assumed fixed, no beta effect
Flow radius, R (km)	37	Radius of curvature around the cape
Flow speed, V (m s^{-1})	0.1, 0.2, 0.3	Speed of flow around the cape
Cross-stream span (km)	13.9	Shear distance estimate
Cross-stream velocity change (m s^{-1})	0.1	Shear velocity change estimate
Angular displacement (°)	90	Arc between straight and curve
Depth at streamline, D (m)	50	Water depth along streamline
(b) Derived parameter (unit)		
Centrifugal acceleration V/R (s^{-1})	$2.7, 5.4, 10.8\times10^{-6}$	Radial acceleration
Across-stream shear, dV/dn (s^{-1})	7.19×10^{-6}	Optional radial shear
Travel time to the cape (s)	$5.8, 2.9, 1.5\times10^{5}$	Vorticity change time
Relative vorticity change (s^{-1})	$0.99, 1.3, 1.8\times10^{-5}$	Vorticity change along stream
Relative vorticity tendency (s^{-2})	$1.7, 4.3, 12.4\times10^{-11}$	Rate of change of vorticity
Vertical velocity grad. dw/dz (s^{-1})	$1.8, 4.6, 12.7\times10^{-6}$	Upwelling velocity gradient
Vertical velocity at depth D (m s^{-1})	$0.87, 2.2, 6.4\times10^{-5}$	Upwelling velocity

prevailing large-scale, low-frequency flow along the continental shelf. Others have studied higher-frequency, quasi-periodic, tidal-frequency flows around capes (Signell and Geyer, 1991; Geyer, 1993; Black et al., 2005; McCabe and MacCready, 2006), but our interest lies in quasi-steady currents and low-frequency variability driven by the wind. Such capes are usually associated with subsurface bathymetric contours that bend and sometimes diverge as they round the cape. Arthur (1965), presented a theoretical development attributed partly to Haltiner and Martin (1957) and others referenced therein. He illustrated the theory using examples obtained from observations of southward flow of the California current around capes off southern California and Baja California. Based on Arthur's theory, Blanton et al. (1981) discussed examples showing northward flow (inshore of the Gulf Stream) around several US east-coast capes, while Kleypas and Burrage (1994) discussed a single (southern hemisphere) example, associated with the flow of the East Australian Current around the southeast tip of the Great Barrier Reef.

The mechanism for induced upwelling or downwelling (which of these occurs depends upon the sign of streamline curvature, the significance of across-stream shear and the strength of the ambient potential vorticity variation), is convergence or divergence of the fluid flow. This allows vortex stretching to adjust its absolute vorticity as it flows around an obstacle, in our case the cape (Arthur, 1965). While in general, vorticity source and sink terms such as wind-stress curl, bottom-boundary stress and horizontal friction may be considered, all the above authors chose to simplify the analysis by considering only the vortex stretching effect of a change in the direction (curvature) of the flow trajectory (following the isobaths). In all the cases considered, the induced response was significant. Restricting our analysis in the same way, we find the possible upwelling response associated with the WAC flow around Cape Gargano under the typical conditions listed in Table 1(a) to be significant (Table 1(b)). In comparison with the cases presented by the other authors, the Cape Gargano case suggests that a modest upwelling response will occur in the region of WAC flow curvature around the cape. The vertical velocity at a depth of 50 m is estimated at 0.87, 2.2, 6.4×10^{-5} m s^{-1} or 0.75, 1.9 and 5.5 m day^{-1} for flow speeds of 0.1, 0.2, 0.3 m s^{-1}, i.e. about 2×10^{-5} m s^{-1} (or ~2 m day^{-1}) for typical horizontal velocities of 0.2 m s^{-1}. These estimates compare well with monthly-averaged and 2-day averaged upwelling velocities of up to 2 m day^{-1} or 5 m day^{-1}, respectively, in the vicinity of the cape, as predicted by the NCOM model (Fig. 14a, b).

While all three sets of authors cited above mentioned isobath divergence as playing a key role in this process, the theory does not seem to demand isobath divergence to generate flow divergence and an associated upwelling response (only isobath curvature seems necessary). It is interesting to distinguish the three cases. That considered by Arthur involved anti-cyclonic flow around a cape, as around Cape Gargano, while the cases considered by Blanton et al. and Kleypas and Burrage involved cyclonic rotation. In the northern hemisphere, anti-cyclonic stream curvature produces upwelling (positive vertical velocity) at depth near the cape (the gradient of vertical velocity is negative, but Arthur's theory assumes the vertical velocity at the surface is zero), while the cyclonic case of Blanton et al. produces a downwelling response. A downwelling response is also produced in the cyclonic case in the southern hemisphere, since the differences in sign of both the Coriolis parameter and the (cyclonic) relative vorticity between the two hemispheres cancel (see Eq. (5), in Arthur, 1965). An interesting complicating feature that is observed in both the Australian and Adriatic cases is the presence of a closed 'lee' eddy in the separation region downstream of the cape. In the presence of bottom-boundary drag, or interfacial drag in the case of stratified flow, bottom Ekman pumping or pycnocline tilt could contribute to, or change the sign of, the upwelling (or downwelling) response. For an unstratified situation typical of winter, bottom Ekman pumping will tend to cause downwelling at the center of an anti-cylonic eddy and, if the eddy is bounded in some way, e.g., by a coast or free shear layer (Wolanski et al., 1996), by upwelling along its periphery (with these locations reversed for a cyclonic eddy). The latter will be reinforced by any upwelling produced by curvature of the boundary current (WAC) main stream, which is assumed to gird the lee eddy. For such cases, the bottom Ekman friction terms need to be included when applying the theory. In its present form the theory implies that, at least in the unstratified season, anti-cyclonic curving streamlines and a persistent anti-cyclonic eddy associated with the WAC flow around Cape Gargano could produce upwelling along the main stream and around the periphery of the eddy, with downwelling in the eddy center and in the WAC further up and downstream of the cape.

The qualitative predictions of this theory are only weakly supported by the DART observational evidence. The NCOM model vertical velocity plots show a persistent upwelling patch off the cape (Fig. 14a, b) and along the outer rims of the mesoscale eddies (Fig. 14c, d) driven by horizontal shear and advection by the WAC, but the small horizontal scale of the patch, in this case, is inconsistent with an assumed flow curvature radius of 37 km, employed in the estimates of Table 1, suggesting that other processes may affect the patch morphology and dynamics. Indeed, in a model bathymetry plot (not shown), the sharp turn in the isobaths, mentioned in Section 7 appears as a ridge extending seaward of the cape. Monthly-averaged vertical velocity plots similar to Fig. 14a, but drawn at progressively deeper depths down to 40 m, show that this ridge marks a transition between an upwelling patch to the west and a downwelling patch to the east, with both patches extending throughout the water column.

This suggests that the upwelling and downwelling patches are caused by the inertial WAC main stream first ascending the ridge on the upstream side, then descending it on the downstream side, while it follows a curved path of larger scale roughly paralleling the coastal outline of the cape. This larger-scale curvature, according to absolute vorticity dynamics should produce upwelling off the cape and downwelling upstream and downstream of the cape. But here, we have upwelling and downwelling patches juxtaposed right near the tip of the cape. The ridge and upwelling/downwelling patches are thus of sufficiently small scale that their dynamics are likely dominated by pressure and form drag effects, rather than absolute vorticity adjustment.

The results of the Aquashuttle survey show upwelling of isotherms (Fig. 9d) in the core of the WAC main stream, but not of isohalines (Fig. 9c). The B75 and B90 SEPTR moorings reveal a mean downwelling response, but only the first of these is close to the 'permanent eddy' center and there is evidence that this effect may be associated with inertial internal waves (Book et al., 2007). Thus, further work is needed to clarify the dynamics of these processes in the vicinity of Cape Gargano, where the implications of changes in other terms of the absolute vorticity such as wind-stress curl and stratification, need to be considered, particularly under transient conditions. Unfortunately, the vertical velocities predicted by both the theory and the NCOM model are much too small ($\sim 10^{-5}$ m s^{-1}) to be directly observed in the field against the background of such processes as internal waves, which exhibit mean downwelling velocities that are about two orders of magnitude larger in magnitude and are significantly larger in scale. Hence further theoretical work is needed to produce appropriate indirect tests of WAC and eddy-induced upwelling that could be used for validating upwelling predictions.

Another perspective on the dynamics of circulation around a cape is afforded by comparison with numerical model results from a comparable hydrodynamic setting. Doglioli et al. (2004) used 2D and 3D numerical hydrodynamic models with both idealized and realistic bathymetry to study the anti-cyclonic coastal current flow around Cape Portofino on the Italian west coast bordering the Ligurian Sea during winter. With moderately high flow, the current separated from the cape and formed a closed recirculation region downstream, which for stronger flows produced eddies that detached and drifted downstream. For the more accurate 3D case, the separation and recirculation were more intense, but also more stable, with less frequent eddy detachment than for the 2D case. They also found a 'secondary' circulation developed consisting of upwelling at the cape near the shelfbreak, fed by offshore flow in the bottom Ekman layer (BEL), with downwelling shoreward (see Doglioli et al., 2004, and their Fig. 11). We computed non-dimensional parameters for Cape Gargano (not shown) and compared them with those computed by Doglioli et al. for Cape Portofino. For the much larger (by a factor of ten) Cape Gargano, the equivalent Reynolds number, Rossby number and Burger number, were all an order of magnitude smaller, while the vertical Ekman number was larger by a factor of three. In comparison with Cape Portofino, Cape Gargano circulation would thus be dominated more by bottom friction and earth rotation (hence, by bottom Ekman layer dynamics), with a consequently stronger upwelling process, while 'turbulence' and stratification would play a lesser role. However, the importance of stratification may be understated by the Burger number, which only represents the bulk vertical density contrast and not the actual gradients. In contrast to Cape Portofino, the reduced gravity off Cape Gargano is an order of magnitude larger with sharper layering (in summer), but Cape Gargano's larger scale (which is an order of magnitude bigger and appears inversely squared in the definition of the Burger number) overwhelms its effect.

The likely ecological impact of the WAC and its associated eddies, filaments and upwelling processes near Cape Gargano will depend upon the extent to which water that is advected horizontally or vertically, along with its constituents, becomes mixed into the receiving waters. Tseng and Ferziger (2001) simulated the effects of coastal geometry and formation of eddies on turbulent mixing in an upwelling zone, using a large-eddy 3D simulation of the Navier Stokes equations based on a rotating circular domain. They found that coherent eddy structures forced by wind were modified in the presence of a cape, which caused strong vortex 'tearing' producing thin filaments extending offshore and downstream. Stirring was enhanced in the cape simulations in comparison with runs conducted without a cape. The results were comparable with features simulated in laboratory experiments and in upwelling circulations observed along the US west coast. Many features of the simulated flows they described appear to have parallels in our observations and modelling results in the vicinity of Cape Gargano; formation of multiple eddies taking the form of a vortex sheet along the WAC front and their evolution into unstable eddies and filaments, and downstream drift and stretching of these features in response to wind forcing and flow around the cape. The correspondence suggests that the attendant vortex stretching, stirring and shear dispersion effects will facilitate across-shelf mixing in the vicinity of the WAC front. Tseng and Ferziger (2001) suggested that with strong stirring and associated development of extensive areas of contact between fluids of differing density or other material properties, irreversible mixing may occur, particularly at the later stages of the evolution of the instabilities. Our in situ data show circumstantial evidence of such mixing in the form of water masses of intermediate salinity and fluorescence following the seasonal thermocline and lying close to interfaces between mesoscale eddies.

9. Conclusions

Meanders and eddies forming along the WAC front, which roughly parallels the Italian east coast, exhibit typical spatial scales of 30 km in remote sensing imagery. The eddies usually show evidence of anti-cyclonic rotation consistent with the prevailing anti-cyclonic across-shelf shear of the along-shelf flow, which is typically stronger offshore. North of Cape Gargano, they tend to form in response to relaxations of the WAC caused by northwestward wind events (or reductions in the strength of southeastward winds). Eddy formation in the vicinity of Cape Gargano tends to follow two distinct patterns. Multiple eddies appearing in response to the Adriatic-wide wind relaxation events just mentioned can form a continuous sequence spanning the coastal regions northwest and southeast of the cape, and spreading along the shelf with an effective crest-to-crest 'wavelength' of 28–37 km. Likely generated by baroclinic instabilities, they may form and dissipate over a period of just a few days in response to transient wind conditions. In contrast to the multiple eddies, isolated eddies may be generated by recirculation of the WAC as it rounds the cape and separates from the coast. These eddies tend to remain stable in the presence of relatively strong and steady WAC flow driven by southeastward winds. Such wind events tend to suppress the formation of the baroclinically unstable multiple eddies, perhaps through the effects of mixed-layer deepening and downwelling near the coast. The MODIS imagery indicates horizontal space and Lagrangian time scales of 18–28 km and 10 days to several weeks, respectively, for the isolated eddies, as they rotate and advect with the mean WAC flow. The NCOM model results show similar time and space scales for these eddies, while the Aquashuttle and current meter mooring data additionally indicate vertical scales of about 20 m pertaining to the summertime stratified season.

The seasonal pattern of meteorological and oceanographic forcing and response predicted by NCOM shows features that are broadly consistent with the specific patterns of eddy variability described above. The model statistics reveal the observed high intensity of mesoscale eddy activity associated with the WAC near Cape Gargano. The monthly mean fields show that this activity is intensified in the summertime stratified season. Mean winds are predominantly

shoreward along the Italian east coast, with a southward tendency that is stronger in summer. Model EKE is strong near the coast, particularly near the cape and to the north, with enhanced eddy activity in a downstream extension southeast of the cape during summer. Wind-stress curl is generally weak and cyclonic in the central Adriatic and immediately northwest of Cape Gargano, but becomes anti-cyclonic along the shelf further to the northwest and also southeast of the cape, where it would tend to reinforce the prevailing anti-cyclonic eddy fields. The pattern of relative vorticity is generally consistent with the above, being broadly cyclonic and weak in the central Adriatic. However Martin et al. (2009) found that NCOM misses significant variance in summer along the Palagruzza Sill, so this weakness may be partly a result of model bias or inaccurate atmospheric forcing. NCOM shows a narrow zone of intense cyclonic vorticity along the outer shelf, particularly in winter. There the WAC flows in deeper water where its intensity may be reduced. Anti-cyclonic rotation prevails along the inner shelf, with the change in sign of the vorticity roughly following the expected across-shelf location of the WAC peak flow.

The instantaneous flows associated with patterns of eddy formation and decay appearing in the observations and model predictions are generally well organized, i.e., they tend to vary smoothly and quasi-periodically, during transition periods between upwelling- and downwelling-favorable wind patterns. However, they sometimes appear chaotic, with relatively short time-scale events (enduring only a few days) characterized by transient formation of off- or on-shore jets, often associated with counter rotating dipole eddies (mushroom jets). Rarely, these events are associated with large-scale changes in the circulation of the central Adriatic, and may be linked to a strong offshore flux of WAC water, such as one that might have crossed to the Croatian side in June, 2006 (see Vilibić, 2009-this issue). More frequently, these jets are of smaller scale, but they still may contribute to significant across-slope exchange. Generation and evolution of mesoscale eddies and filaments present a special challenge for coastal modeling and prediction in the Adriatic Sea. There is high temporal and spatial variability in its wind fields and the orography, coastal outline and bathymetry are relatively complex. Thus, high-resolution data are required to specify the meteorological and geometric fields with sufficient accuracy for Rapid Environmental Assessment applications. Ocean stratification also plays a significant role, particularly in summer, when development of baroclinic instabilities along the WAC front appears commonplace, yet stratification cannot be directly studied using remote sensing data. Features that may be locally intense can form, deform, advect and/or disperse quite rapidly, so rapid sampling and fine spatial and temporal resolution are required when acquiring in situ data for simulation model initialization, assimilation or validation. Visible and infra-red remote sensing imagery is useful to characterize typical responses of the coastal ocean to varying meteorological forcing conditions, but acquisition of long time series is inhibited by cloud cover, especially in winter. Numerical hydrodynamic models can help fill gaps by providing more continuous descriptions of eddy kinematics, and they also help to elucidate the underlying dynamics. Model sensitivity to initial conditions and to small perturbations due to small numerical errors or variations in the specification of boundary conditions also poses a special challenge. As a result, the best models will typically reveal the character, but not the precise details, of flow evolution. On the other hand, strong topographic constraints can localize flow features and increase flow stability, and thus enhance the spatial accuracy of circulation models.

Qualitative analysis of the results and judicious use of dimensional analysis can help to identify and locate key features and processes of operational or ecological significance that could be targeted in future coastal monitoring efforts. Our analysis shows that an isolated eddy that frequently forms downstream of Cape Gargano under moderately strong and sustained WAC flows may be associated with persistent upwelling along the WAC main stream as it rounds the cape and encircles the eddy. Such a feature could be identified and tracked using remote sensing imagery in combination with data from a small number of strategically located monitoring stations. The multiple-eddy sequences that form during WAC flow relaxation events are temporally less predictable and thus more difficult to resolve using in situ data. However, their coherent and quasi-periodic spatial structure could be exploited to develop models of their distribution and impact that rely on a few key monitoring station locations to predict the overall pattern.

This paper has demonstrated that combined use of remote sensing imagery and numerical model simulations, validated by in situ data, can yield a more comprehensive view of complex coastal circulation processes than is possible with any of these data sources, considered alone. Using the remote sensing data acquired during DART, we demonstrated that satellite sea surface temperature (SST) and chlorophyll-*a* (Chl-a) imagery from the Aqua/Terra MODIS sensors reveals two distinct cases of WAC eddy activity in the vicinity of Cape Gargano. In the first case, a single anti-cyclonic circulation cell forms on the downstream side of the cape. This single eddy may grow in size and ultimately detach from the cape to advect southeastward in the prevailing current. In the second case, a sequence comprising multiple eddies may evolve over the long straight stretch of coast beginning upstream and proceeding around the cape. Our analysis of simulation results obtained using the DART regional implementation of the NCOM numerical hydrodynamic model suggests that these distinct cases are associated with variations in the strength of the WAC that are driven by temporal variations in the strength and direction of the prevailing wind. It has also shown that the model provides plausible predictions of surface current, temperature and salinity fields that show fair qualitative agreement with surface fields derived from in situ data and satellite imagery in the presence of complex mesoscale eddy fields. We have found that due to their connection with large-scale wind patterns, the general timing and region of development of mesoscale eddies and filaments in the WAC may be predicted using realistic ocean models, such as NCOM. However, predicting most of the details of these features such as their precise timing, location and shape, remains an open challenge for the implementation of Rapid Environmental Assessment procedures.

Acknowledgements

Outstanding ship operations and support from the captains, crews and scientists of R/V G. Dallaporta, R/V Alliance, and R/V Universitatis for instrument deployment and recovery during the Dynamics of the Adriatic in Real Time (DART) experiments are gratefully acknowledged. The success of the field work, including extensive instrument deployment and recovery operations, was greatly facilitated by the dedicated efforts of Mark Hulbert, Andrew Quaid, and Wesley Goode of the NRL technical team. Michel Rixen of the NATO Undersea Research Centre (NURC) led and organized the larger international DART collaborative project and contributed in many ways to the work. The NRL DART project greatly benefited from participation in the NURC/NRL Joint Research Project and from contributions by many international partners. ALADIN wind products were provided by Martina Tudor through the Croatian Meteorological and Hydrological Service. The SEPTR moorings were developed through a cooperative agreement between NRL and NURC and we thank Vittorio Grandi, Lavinio Gualdesi, Alessandro Carta, and Emanuel Coelho for their contributions. Po River discharge data were provided courtesy of ARPA-SIM Emilia Romagna. David Walsh developed the initial AquaShuttle software and processed the wintertime data. Remote sensing images were acquired from NASA and processed by Sherwin Ladner of Planning Systems Incorporated at NRL, Stennis Space Center. A summer student, Aspen Nero assisted with the compilation, editing and interpretation of these images through the Science and

Engineering Apprentice Program of the American Society of Engineering Education. This work was supported by the Office of Naval Research as part of the "Dynamics of the Adriatic in Real Time" and the "Global Remote Littoral Forcing via Deep Water Pathways" research programs under Program Element Numbers 0602435N and 0601153N, respectively. This is NRL contribution NRL/JA/7330-08-8152.

References

Artegiani, A., Bregant, D., Paschini, E., Pinardi, N., Raicich, F., Russo, A., 1997a. The Adriatic Sea general circulation. Part I: Air–Sea Interactions and Water Mass Structure. J. Phys. Oceanogr. 27, 1492–1514.

Artegiani, A., Bregant, D., Paschini, E., Pinardi, N., Raicich, F., Russo, A., 1997b. The Adriatic Sea general circulation. Part II: Baroclinic Circulation Structure. J. Phys. Oceanogr. 27, 1515–1532.

Arthur, R.S., 1965. On the calculation of vertical motion in eastern boundary currents from determination of horizontal motion. J. Geophys. Res. 70 (12), 2799–2803.

Barron, C.N., Kara, A.B., Hurlburt, H.E., Rowley, R.C., Smedstad, L.F., 2004. Sea surface height predictions from the global Navy Coastal Ocean Model (NCOM) during 1998–2001. J. Atmos. Ocean. Technol. 21 (12), 1876–1894.

Black, K., Oldman, J., Hume, T., 2005. Dynamics of a 3-dimensional, baroclinic, headland eddy. N. Z. J. Mar. Freshw. Res. 39, 91–120.

Blanton, J.O., Atkinson, L.P., Pietrafesa, L.J., Lee, T.N., 1981. The intrusion of Gulf Stream water across the continental shelf due to topographically-induced upwelling. Deep-Sea Res. 28A(4), 393–405.

Book, J.W., Perkins, H.T., Cavaleri, L., Doyle, J.D., Pullen, J.D., 2005. ADCP observations of the western Adriatic slope current during winter of 2001. Prog. Oceanogr. 66, 270–286.

Book, J.W., Rixen, M., Martin, P.J., Burrage, D., 2007. Observations of the western Adriatic current as a summertime mixed-layer system. Abstract, Poster Paper, Rapid Environmental Assessment Conference, 25–27 Sept., Lerici, Italy.

Burrage, D.M., Steinberg, C.R., Skirving, W.J., Kleypas, J.A., 1996. Mesoscale circulation features of the Great Barrier Reef region inferred from NOAA satellite imagery. Remote Sens. Environ. 56, 21–41.

Cushman-Roisin, B., Gačić, M., Poulain, P.-M., Artegiani, A. (Eds.), 2001. Physical Oceanography of the Adriatic Sea: Past, Present and Future. Springer, New York. 304 pp.

Cushman-Roisin, B., Korotenko, K.A., Galos, C.E., Dietrich, D.E., 2007. Simulation and characterization of the Adriatic Sea mesoscale variability. J. Geophys. Res. 112 (C03S14), 1–13. doi:10.1029/2006JC003515.

Denniss, T., Middleton, J.H., Manasseh, R., 1995. Recirculation in the lee of complicated headlands: a case study of Bass Point. J. Geophys. Res. 100 (C8), 16087–161010.

Doglioli, A.M., Griffa, A., Magaldi, M.G., 2004. Numerical study of a coastal current on a steep slope in presence of a cape: The case of the Promontorio di Portofino. J. Geophys. Res. 109 (C12033). doi:10.1029/2004JC002422.

Geyer, W.R., 1993. Three-dimensional flow around headlands. J. Geophys. Res. 98 (C1), 955–966.

Gregg, M.C., Hess, W.C., 1985. Dynamic response of Sea-Bird temperature and conductivity probes. J. Atmos. Ocean. Technol. 2, 304–313.

Haltiner, G.J., Martin, F.L., 1957. Dynamical and Physical Meteorology. McGraw-Hill, New York, p. 470.

Horne, E.P.W., Toole, J.M., 1980. Sensor mismatches and lag correction techniques for temperature–salinity profilers. J. Phys. Oceanogr. 10, 1122–1130.

Hu, C., Carder, K.L., Muller-Karger, F.E., 2000. Atmospheric correction of SeaWiFS Imagery over turbid coastal waters: A practical method. Remote Sens. Environ. 74, 195–206.

Ivatek-ahdan, S., Tudor, M., 2004. Use of high-resolution dynamical adaptation in operational suite and research impact studies. Meteorologische Zeitschrift 13, 1–10.

Kleypas, J.A., Burrage, D.M., 1994. Satellite observations of circulation in the southern Great Barrier Reef, Australia. Int. J. Remote Sens. 15, 2051–2063.

Korotenko, K.A., 2007. Modeling the mesoscale variability of the Adriatic Sea. Oceanology 47 (3), 340–353.

Lueck, R.G., 1990. Thermal inertia of conductivity cells: theory. J. Atmos. Ocean. Technol. 7 (5), 741–755.

Lueck, R.G., Picklo, J.J., 1990. Thermal inertia of conductivity cells: Observations with a Sea-Bird cell. J. Atmos. Ocean. Technol. 7 (5), 756–786.

Mahadevan, A., Thomas, L.N., Tandon, A., 2008. Comment on "Eddy/wind interactions stimulate extraordinary mid-ocean plankton blooms". Science 320, 448b.

Martin, P.J., 2000. A Description of the Navy Coastal Ocean Model Version 1.0 NRL Report NRL/FR/7322 00-9962, Naval Research Laboratory, SSC, MS 39529, 42 pp.

Martin, P.J., Book, J.W., Doyle, J.D., 2006. Simulation of the northern Adriatic circulation during winter 2003. J. Geophys. Res. 111, C03S12. doi:10.1029/2006JC003511.

Martin, P.J., Book, J. W., Burrage, D.M., Rowley, C.D., Tudor, M., 2009. Comparison of model-simulated and observed currents in the central Adriatic during DART, J. Geophys. Res. 114, C01S05. doi:10.1029/2008JC004842.

McCabe, R.M., MacCready, P., 2006. Form drag due to flow separation at a headland. J. Phys. Oceanogr. 36, 2136–2152.

Morison, J., Andersen, R., Larson, N., D'Asaro, E., Boyd, T., 1994. The correction of thermal-lag effects in Sea-Bird CTD data. J. Atmos. Ocean. Technol. 11, 1151–1164.

Munday, D.R., Marshall, D.P., 2005. On the separation of a barotropic western boundary current from a cape. J. Phys. Oceanogr. 35, 1726–1743.

Orlić, M., Gaić, La Violette, P.E., 1992. The currents and circulation of the Adriatic Sea. Oceanol. Acta 15, 109–124.

Pacheco, M., Garcia-Weil, L., Rodriguez, G.R., Tejera, A., Luque, A., 2001. Upwelling filaments in the Northwest African Coastal Transition Zone (NACTZ); satellite images and laboratory simulations. IGARSS '01 IEEE 2001, 9–13 July, 2001, Sydney, NSW, Australia, Proceedings, vol. 7, pp. 3015–3017. doi:10.1109/IGARSS.2001.978239.

Pasari, Z., Belušić, D., Klaić, Z.B., 2007. Orographic influences on the Adriatic sirocco wind. Ann. Geophys. 25, 1263–1267.

Pasari, Z., Belušić, D., Chiggiato, J., 2009. Orographic effects on meteorological fields over the Adriatic from different models. J. Mar. Systems 78, S90–S100 (this issue).

Perkins, H., de Strobel, F., Gualdesi, L., 2000. The Barny Sentinel Trawl-Resistant ADCP bottom mount: Design, Testing, and Application. IEEE J. Ocean. Eng. 25 (4), 430–436.

Poulain, P.-M., 2001. Adriatic Sea surface circulation as derived from drifter data between 1990 and 1999. J. Mar. Syst. 29, 3–32.

Raicich, F., 1994. Note on the flow rates of the Adriatic rivers. IST-CNR Tech. Rep. RF-02/94 (Italy).

Raicich, F., 1996. On the fresh water balance of the Adriatic Sea. J. Mar. Syst. 9 (1–2), 305–319.

Signell, R., Geyer, W.R., 1991. Transient eddy formation around headlands. J. Geophys. Res. 96 (C2), 2561–2575.

Takahashi, D., Kazuo, K., Yoshinori, N., Kobayashi, N., Higaki, N., Hideo, M., 2007. Dynamical structure and wind-driven upwelling in a summertime anticyclonic eddy within Funka Bay, Hokkaido, Japan. Cont. Shelf Res. 27 (14), 1928–1946.

Tseng, Y.H., Ferziger, J.H., 2001. Effects of coastal geometry and the formation of cyclonic/anti-cyclonic eddies on turbulent mixing in upwelling simulation. J. Turbulence 2 (014), 23.

UNESCO, 1983. Algorithms for Computation of Fundamental Properties of Seawater. Technical Papers in Marine Science, vol. 44. UNESCO Division of Marine Science, Paris. 53 pp.

Vilibić, I., Book, J.W., Beg Paklar, G., Orlić, M., Dadić, V., Tudor, M., Martin, P.J., Pasarić, M., Grbec, B., Matić, F., Mihanović, H., Morović, M., 2009. West Adriatic coastal water excursions into the East Adriatic. J. Mar. Systems 78, S132–S156 (this issue).

Wolanski, E., Takashi, A., Akihiro, T., Deleersnijder, E., 1996. Three-dimensional island wakes in the field, laboratory experiments and numerical models. Cont. Shelf Res. 16 (11), 1437–1452.